

**Short-term Wind Resource Forecasting for the Wind Farm,
Under the Influence of Extreme Seasonal Variations and
Inter-Farms Wake**



By

Raja Muhammad Asim Feroz

Reg # 00000206014

Session 2017-2019

Supervised by

Dr. Adeel Javed

**A Thesis Submitted to the US Pakistan Centre for Advanced
Studies in Energy in partial fulfillment of the requirements of the
degree of**

MASTER of SCIENCE

in

THERMAL ENERGY ENGINEERING

**US-Pakistan Centre for Advanced Studies in Energy
(USPCAS-E)**

**National University of Sciences and Technology (NUST) H-12,
Islamabad 44000, Pakistan**

July 2020

THESIS ACCEPTANCE CERTIFICATE

Certified that final copy of MS thesis written by Raja Muhammad Asim Feroz (Registration No. 00000206014), of U.S.-Pakistan Centre for Advanced Studies in Energy has been vetted by undersigned, found complete in all respects as per NUST Statues/Regulations, is within the similarity indices limit and accepted as partial fulfillment for the award of MS/MPhil degree. It is further certified that necessary amendments as pointed out by GEC members of the scholar have also been incorporated in the said thesis.

Signature: _____

Name of Supervisor: Dr. Adeel Javed

Date: _____

Signature (HOD): _____

Date: _____

Signature (Dean/Principal): _____

Date: _____

Certificate

This is to certify that work in this thesis has been carried out by **Mr. Raja Muhammad Asim Feroz** and completed under my supervision in, US-Pakistan Center for Advanced Studies in Energy (USPCAS-E), National University of Sciences and Technology, H-12, Islamabad, Pakistan.

Supervisor:

Dr. Adeel Javed
USPCAS-E
NUST, Islamabad

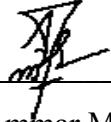
GEC member # 1:

Dr. Adeel Waqas
USPCAS-E
NUST, Islamabad

GEC member # 2:

Dr. Majid Ali
USPCAS-E
NUST, Islamabad

GEC member # 3:



Dr. Ammar Mushtaq
RCMS
NUST, Islamabad

HOD-Thermal Energy Engineering:

Dr. Adeel Javed
USPCAS-E
NUST, Islamabad

Principal/ Dean:

Dr. Adeel Waqas
USPCAS-E
NUST, Islamabad

Acknowledgments

All praise to Allah Almighty who gave me the strength and knowledge to do the work presented in this thesis.

I would like to acknowledge the profound supervision and guidance of Dr. Adeel Javed throughout this research and thesis. His professional approach towards a problem can only be surpassed by his friendly supervision that has brought best out of me. He polished my research skills and I have learned a lot under his supervision and guidance.

I would also like to thank the members of my GEC committee, Dr. Majid Ali, Dr. Adeel Waqas, and Dr. Ammar Mushtaq who honored my committee's presence. I would also acknowledge the High-Performance Computing facility at U.S.-PCASE for providing me the space to carry out comprehensive simulations involved in this work.

This research work was not possible without the technical support provided by the three wind power plants: FFCEL Energy Ltd., Zorlu Energy Ltd., Three Gorges First Windfarm Ltd. and Master Wind Energy Ltd. I want to especially acknowledge Mr. Zeeshan Shafique, Head of Technical FFCEL, for all the guidance and technical data provided.

Abstract

Wind forecasting for the commercial-scale wind farm is vital for grid management issues, energy trading, tariff adjustment, and maintenance issues. Forecasting of the wind farm located in the complex terrain causes a major challenge. The challenge for the prediction of wind resources for that wind farm immensely increases if inter-farm wakes affect wind farms and under the severe variations of seasonal changes. The Weather Research and Forecasting (WRF) model is used for the mesoscale wind resource forecasting for the wind farm under the effect of immense and complex wakes from neighboring wind farms. The test case wind farm is located in the complex terrain of the Jhimpir wind corridor, Sindh, Pakistan. Simulation for forecasting was done for two cases i.e. Without inter-farm wakes and With Inter-farm wakes, during the prediction of wind resources for the wind farm. A significant reduction in error assessment parameters has been observed for Case 2. For the month of June (Summer), the mean absolute errors in wind speed prediction were reduced by 7.7 %. In the month of January (Winter), 14 % of error reduction in mean absolute error was observed. The power predicted was improved by 15 % and 26 %, for June and January, respectively. However, the forecasting skill of the WRF is deteriorated in the winter. The Pearson correlation factor assesses the forecasting skill of the WRF for wind power prediction, the value of correlation in June is 0.82 and for winter its value is 0.27.

Keywords: wind farm; energy forecasting; wake interference; seasonal variation; mesoscale simulation

Table of Contents

| | |
|---|-----------|
| Chapter 1 Introduction | 1 |
| 1.1 Motivation | 1 |
| 1.2 Case Study | 2 |
| 1.3 Objectives | 3 |
| 1.4 Thesis Outline..... | 4 |
| Chapter 2 Literature Review | 7 |
| 2.1 Techniques of Wind Speed Forecasting | 8 |
| 2.1.1 Statistical Methods | 8 |
| 2.1.2 Physical Methods | 8 |
| Chapter 3 Wind farms specification and WRF configuration | 15 |
| 3.1 Wind Farm Parameters | 15 |
| 3.2 WRF Model Configuration | 16 |
| 3.3 Simulation Setup | 18 |
| Chapter 4 WRF Model Validation | 23 |
| 4.1 Error Parameters | 23 |
| Chapter 5 Results and Discussion | 27 |
| 5.1 Wind speed and Direction analysis | 27 |
| 5.2 Error Analysis of turbines | 30 |
| 5.2.1 Mean Absolute Error..... | 30 |
| 5.2.2 Root Mean Square Error | 33 |
| 5.3 Power Prediction Analysis | 34 |
| 5.3.1 Normalized Mean Absolute Error..... | 36 |
| Chapter 6 Conclusions | 40 |
| 6.1 Conclusions | 40 |
| 6.2 Future Research Work..... | 41 |
| Chapter 7 Research exchange Work | 43 |
| 7.1 Lidar Lab in ASU | 43 |
| 7.1.1 Ultra-Sonic Anemometer | 43 |
| Chapter 8 Appendices | 45 |

List of Figures

| | |
|--|-----------------------------|
| Figure 1.1 The FFCEL Wind Farm located in the Jhimpir wind corridor..... | 2 |
| Figure 1.2 Methodology applied for the current study..... | 3 |
| Figure 3.1 Layout of the FFCEL wind farm with neighboring wind farm | 15 |
| Figure 3.2 a) Wind farm layout | b) WRF model nested domains |
| | 17 |
| Figure 3.3 Wind farm layout, categorizing wind turbines in two sets i.e. A: with less intra-farm spacing between wind turbines, B: With more intra-farm spacing between them..... | 18 |
| Figure 5.1 Temporal variation between forecasted (without and with inter-farm wake effects) and observed wind speed for the first week in months of (a) June, (b) July, and (c) January..... | 27 |
| Figure 5.2 Speed deficit is observed due to the Inter farm wakes for both cases, Case 1: without Inter-farm wakes, Case 2: With inter-farm wakes, Approx. 1 ms^{-1} of wind speed deficit is observed due to upstream wind farm | 28 |
| Figure 5.3 Comparison of predicted wind direction with observed values for the months of (a) June, (b) July, and (c) January..... | 29 |
| Figure 5.4 Comparison of mean absolute errors (MAE) of wind speed experienced by individual turbines for Case 1: Without inter-farm wake effects and Case 2: With inter-farm wake effects for (a) June, (b) July, and (c) January. Error values are higher in January as compared to the summer months..... | 30 |
| Figure 5.5 Wind speed forecasting analysis for the month of June, set A turbines is represented in (a) turbine 1, (b) Turbine 3, (c) Turbine 11, where (d)Turbine 16, (e) Turbine 22, (f) Turbine 31 represent set B turbines, Δ represents the reduced in MAE in ms^{-1} , where R1 and R2 represents the Pearson correlation for Case 1 and Case 2, respectively | 31 |
| Figure 5.6 Wind speed forecasting analysis for the month of January, set A turbines is represented in (a) turbine 1, (b) Turbine 3, (c) Turbine 11, where (d)Turbine 16, (e) Turbine 22, (f) Turbine 31 represent set B turbines, Δ represents the reduction in MAE in ms^{-1} , where R1 and R2 represents the Pearson correlation for Case 1 and Case 2, respectively | 32 |
| Figure 5.7 Comparison of root mean square error (RMSE) values of wind speed experienced by individual turbines for Case 1: Without inter-farm wake effects and Case 2: With inter-farm wake effects for (a) June, (b) July, and (c) January. | 33 |
| Figure 5.8 Comparison of forecasted and observed total power generation in FFCEL for Case 2: With inter-farm wake effects for the months of (a) June, (b) July, and (c) January..... | 34 |
| Figure 5.9 Wind power forecasting analysis for the month of June, set A turbines is represented in (a) turbine 1, (b) Turbine 3, (c) Turbine 11, where (d)Turbine 16, (e) Turbine 22, (f) Turbine 31 represent set B turbines, Δ represents the reduction in % deficit reduction in normalized power prediction | 35 |

| | |
|--|----|
| Figure 5.10 Wind power forecasting analysis for the month of January, set A turbines is represented in (a) turbine 1, (b) Turbine 3, (c) Turbine 11, where (d) Turbine 16, (e) Turbine 22, (f) Turbine 31 represent set B turbines, Δ represents the reduction in % deficit reduction in normalized power prediction | 36 |
| Figure 5.11 Comparison of normalized mean absolute error values, (NMAE) in %, of power generated by individual turbines for Case 1: without inter-farm wake effects and Case 2: With inter-farm wake effects..... | 37 |
| Figure 5.12 Comparison of predicted and observed total power generation of FFCEL for the months of (a) June, (b) July, and (c) January..... | 38 |
| Figure 7.1 (a) Fabricated ultrasonic anemometer (b) Testing in the wind tunnel..... | 43 |
| Figure 7.2 Speed variation ultrasonic anemometer with actual data | 44 |

List of Tables

| | |
|---|----|
| Table 3.1 Wind Farm specification of the FFCEL with neighboring wind | 16 |
| Table 3.2 Detail of domains and grid points | 17 |
| Table 3.3 Simulation design for two cases i.e. Without Inter-farm and With Inter-farm wakes..... | 18 |
| Table 4.1 Statistical Error analysis for both cases..... | 24 |

Nomenclature

| | | | |
|----------------------|---|-------|--|
| Variables | | TGF | Three Gorges wind farm |
| <i>Obs</i> | Observed values | MW | Megawatt |
| <i>f</i> | forecasted values | GFS | Global Forecasting System |
| <i>n</i> | total number of observations | NCEP | National Center for Environmental Prediction |
| <i>dx</i> | horizontal resolution | MODIS | Moderate Imaging Spectroradiometer |
| <i>dy</i> | vertical resolution | MYNN | Mellor–Yamada Nakanishi Niino |
| | | PBL | Planetary boundary layer |
| Abbreviations | | MAE | Mean Absolute Error |
| GW | gigawatt | MBE | Mean Bias Error |
| CFD | Computational Fluid Dynamics | RMSE | Root Mean Square Error |
| NWP | Numerical Weather Prediction | NMAE | Normalized Mean Absolute Error |
| MM5 | Mesoscale Model | R | Pearson Correlation Coefficient |
| LES | Large-eddy Simulation | UTC | Coordinated Universal Time |
| WRF | Weather Research and Forecasting | kW | kilowatts |
| FFCEL | Fauji Fertilizer Company Energy Limited | | |

Chapter 1

Introduction

1.1 Motivation

Conventional fossils have been the sole sources of energy for many years until the research in the alternative sources had broken through. With the increase in the efficiency, alternative sources of energy, which is commonly called renewable sources, gain special attention due to global concern on the depletion of the conventional source of energy and global warming. International countries have agreements such as the Kyoto Protocol, in which member countries are committed to providing certain percent of their energy demands with renewable [1]. Wind energy gained an important source of power production among all the renewable sources of energy, due to advancements in research and technology in the wind sector. Global wind-generation installed capacity has increased by the factor of 75 over the two decades, from 7.5 GW in 1997 to 664 GW in 2018 [2]. The power sources of wind energy around the world including the US are in the complex terrain due to flow enhancement and channeling by the topographic features[2]. However, before integrated those power into the national grids, accurate estimation of potential contribution is necessary to ensure efficient utilization [3]. Therefore, accurate atmospheric modeling about complex terrain is necessary for forecasting wind production.

Unlike other sources of renewable sources, wind energy has peculiar characteristics, it changes with the spatial, diurnal, seasonal, and temporal variations. Also, unlike the traditional source of energy, intermittency of wind energy poses a huge challenge for wind energy resource planners. Wind energy forecasting is very essential for grid maintenance timing, day-ahead energy trading in the market, reducing the imbalance between charges and penalties, and efficient project management issues.

In 2013, Pakistan meteorological Department conducted a survey entitled “Wind potential survey in the coastal area of Pakistan”. That study was funded by the Ministry of Science and Technology. That study proposed the “Gharo-Jhimpir region” as the economically feasible areas to established wind farms after this study number of wind farms establishing

in that region is increasing. With the increase in wind farms numbers, the need to provide accurate wind resource for the wind farms under the influence of inter-farm wakes is the challenge, that wind farms are facing.

1.2 Case Study

In 2013, the Meteorological Department of Pakistan (PMD) conducted a survey entitled “Wind Power Potential Survey of Coastal Areas of Pakistan”, funded by the Ministry of Science and Technology. That study enabled PMD to identify the potential “wind



Figure 1.1 The FFCEL Wind Farm located in the Jhimpir wind corridor

corridors” where economically feasible could be established. The Gharo-Jhimpir wind corridor in Sindh was identified as the most lucrative site for wind power plants. The wind power potential covered an area of 9700 sq.km with a gross wind power potential of 43000 MW. The test case wind farm is the Fauji Fertilizer Company Energy Limited (FFCEL) wind farm, which is situated in the Jhimpir Corridor shown in Fig 1.1, The FFC wind farm is operational since 2013. It has a production capacity of 49.5 MW. It contains 33 wind turbines of Nordex S 77 with each having the 1500 KW maximum power. All the wind farms are now under the influence of wakes from the neighboring wind farms.

wakes from the upstream wind farms cause loss of power production in downstream farms.

In this study, I forecasted the wind resources for the wind farm, which is under the influence of intra and inter farm wakes. That wind farm is prone to the extreme seasonal variation throughout the year. These factors make this study one of its kind for the wind speed and power forecasting for a wind farm. The mesoscale Numerical Weather Prediction (NWP), Weather Research and Forecasting (WRF) are used with the Wind Farm Parametrization scheme to estimate the wind farms' wakes.

1.3 Objectives

This study was carried out to achieve the following objectives

- a. short-term wind forecasting of the wind farm under the influence of inter-farm wakes
- b. total power prediction of the wind farm
- c. evaluation of variation in wind speed by the seasonal changes
- d. error analysis in power prediction by individual turbines

the methodology which was used in this study is shown in Fig. 1.2. The Time-dependent data, Geographical data, and Wind turbines data serve the inputs for the WRF model. After the WRF model is set, two types of simulations were designed to run i.e. without interfarm wake and with interfarm wake. Then the predicted output of the WRF is compared with

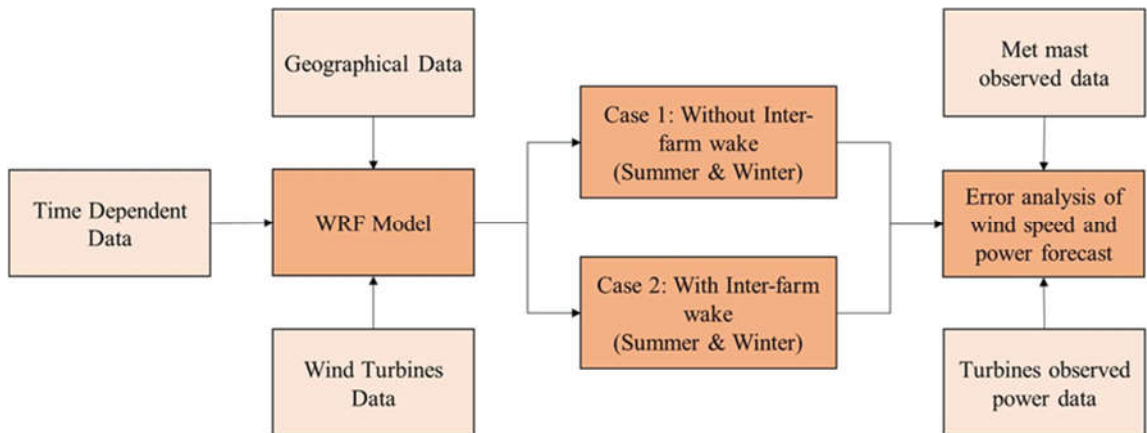


Figure 1.2 Methodology applied for the current study

the observed data of wind speeds from the met mast and wind turbines, and power data of wind turbine of the wind farm

1.4 Thesis Outline

The following is a summary of the different chapters in this thesis.

Chapter 2 discusses the different forecasting models and techniques used by the scientific community to predict wind resource estimation. This chapter also discusses the different forecasting models for the wind speed and power forecasting of a wind farm. The WRF mesoscale model is discussed, the pros and cons of different technique of forecasting are also discussed

Chapter 3 describes the FFCEL wind farm and the neighboring wind farms specifications. The WRF parameters which are used are also discussed along with the design of simulations for the study

Chapter 4 includes the validation of the WRF results with observed values of met mast and wind farm. Different statistical parameters are assessed for the errors in wind speed and power

Chapter 5 discusses the results of the study. The effects of inter-farm wakes on the wind speed forecasting are discussed. Changes in the wind direction in different seasons are analyzed. Errors emerge from neglecting inter-farm wakes in each wind turbine is discussed. Total power of the wind farm is estimated in different cases

Chapter 6 conclusions, which are drawn from the study are included in this chapter. It also discusses the future studies emerges from this study

Chapter 7 discusses the author's research work during his semester-long exchange program at Arizona State University (ASU), USA.

Summary

Over the last decade, the number of wind farms has been establishing in the Jhimpir wind corridor, Pakistan, this raises the problem of wind forecasting of the wind farm under the influence of inter-farm wakes from the neighboring wind farms. The Jhimpir lies in the complex region and experiences extreme seasonal variation around the year. This factor makes prediction of wind resources for the test case wind farm in Jhimpir a new case to study.

References

- [1] B. Ki-moon, “Kyoto Protocol Reference Manual,” *United Nations Framew. Conv. Clim. Chang.*, p. 130, 2008.
- [2] IRENA, *Renewable Energy Statistics 2019*, vol. 1, no. 1. 2019.
- [3] M. Martín, L. V. Cremades, and J. M. Santabàrbara, “Analysis and modelling of time series of surface wind speed and direction,” *Int. J. Climatol.*, vol. 19, no. 2, pp. 197–209, 1999.

Chapter 2

Literature Review

In the past, various studies have been done to predict wind energy for wind farms and sites all over the globe. In Jamaica, a random probability distribution was made from the past data, and time series were then tested with the observed data [1]. Wind speed was forecasted for the aa wind turbines in the Pomeroy, Iowa wind farm, USA [2]. By coupling mesoscale model with microscale is another very innovative way to forecast i.e. coupling mesoscale model with CFD was used to predict the wind speed in the Nygaard, Norway and also coupling Windsim with the mesoscale was used for wind prognostication of the wind farm in Manisa, Turkey [3]-[4]. A hybrid method, coupling physical method with the statistical method is also used by some scientists to predict the wind speed. Kalman filter and genetic algorithm as the statistical methods with the physical method were used for the wind characteristics prediction in Japan and Spain, respectively [5]-[6]. These studies include wind speed prediction from a 24 to 72h forecast horizon. These studies did not include inter-farm wake for the wind speed prediction.

Upstream wind farms produce wakes, these wakes cause the loss in the power in the downstream wind turbines. These wakes are imminent as wind farms are established with the minimum distance between them due to the cost and land constraints. Wakes from the utility-scale wind turbines persist for 8-10 diameter of that turbine [7]. As wakes can cause a loss in the power production of wind turbines, hence it can lead to an increase in the cost of electricity generations. Wind farm optimization is done by Jonas et al. [8], used three different models to propose optimal horizontal distance between turbines, for these intra-farm wakes to get a minimum. [9] used different flow cases to find the wake effects of neighboring wind turbines, he analyzed the effect of the wake is maximum on the downstream wind turbines that are directly in front of upstream wind turbines. The analytical modeling of the wind turbine was done to estimate the velocity distribution behind the wind turbine is done by [10]. Two different techniques were carried by [11] to analyze the wakes of neighboring wind turbines. Gonzalez et al. [12] proposed the

nature of wind turbine used and spacing between wind turbines can affect wind farm efficiency.

A wind speed forecasting for a wind farm neglecting the inter-farm wakes could give an overestimation of speed, which leads to large errors in power output because of cubic relation between speed and power. Even a small error in wind speed could increase to three times in the power estimation [13]. [14] analyzed the wind speed forecasting catering the intra-farm wakes on the real onshore wind farm, he discovered 0.5% loss in wind resource even after 17 km behind wind farm. [15] proposed that a 35 % loss in power prediction due to the wake effect of upstream wind turbines. Both intra- and-inter-farm wake flows affect wind resources by different wind turbine s in an onshore wind farm. Due to land constraints, wind farms are developed uncoordinated with less than the nominal distance between them, thus give large errors in wind power prediction. Spatial and geographical parameters should be catered as these parameters affect the atmospheric boundary layer while prediction wind speed forecasting.

2.1 Techniques of Wind Speed Forecasting

2.1.1 Statistical Methods

There are mainly two techniques for wind speed forecasting i.e. statistical methods and physical methods. Statistical models are used to predict wind speed for very short-term prediction. These models are auto recursive, these models tune their parameters based on the difference between predicted and original values c. Such studies include forecasting using Kalman filters [17], ARMA (Auto Regression Moving Average) functions [18], functions using neural networks [19]-[20], the fuzzy logic method [21], and Box-Jenkins models [1]. The Forecasting skills depend on the reliability of the past data and the number of points in that data [22], [23] demonstrated difficulties of using past data in wind speed forecasting. As the lead time increases the error in wind speed forecasting increases.

2.1.2 Physical Methods

For the wind speed forecasting more than 6hrs time horizon, there is another method which gives an excellent first approximation of wind resource estimation i.e. Numerical Weather Prediction (NWP) models [24]-[25]. NWP models use meteorological data for wind speed forecasting [26]. NWP models are very effective, as these models solve

conservation of mass, energy, heat, and momentum equations on a real location and geographical grid points in the three dimensions. These models also include the effect of latitude, longitude, and topography of the location. NWP models have certain merit over statistical methods, these can scale downwind speed to the hub-height of the wind turbine, do not have missing data and give high resolution in horizontal and vertical domains [27]-[28]. These models can be used for the wind farm layout and power curve of wind turbines in the wind farm. NWP models use interpolation techniques to scale down the wind speed, accounting for the description of the terrain. Collecting terrain information is rather a difficult task. Modeling techniques to estimate wind speed now are more and more accurate. NWP models are run on supercomputers, as they require immense computational power [29].

2.1.2.1 WRF

Wind farm characterization can be used in current modeling tools that used atmospheric interaction with the wind farm in their simulations. The WRF [30] is the current state of the art modeling tool, which is developed on the MM5 model. It uses terrain information and eulerian based specification for the particle flow in wind resource forecasting. WRF uses microphysics parametrization schemes, long and short-wave radiations, planetary boundary layer, cumulus process, and surface processes, to enhance the interaction of the atmosphere with the terrain. These models use physical parametrization to resolve the complex process and predict temperature, wind speed, and water vapor over the three dimensions[31]-[32]. [2] and [33] used the WRF to predict wind speed turbine-hub height. The WRF has the excellent capability to predict wind speed over the complex terrain [28], [34]-[35]. Like other NWP, the WRF can perform simulation less than few hundred meters, Large-eddy simulation (LES) has proven to be the very effective technique used for the wind farm characterization and estimation of the turbulent phenomena and its mixing and its effect on the wind farm [10], [36]-[37]. Although, LES [38] has excellent ability to resolve the wake phenomena but they require extensive computational power, that is why LES has not been very effective for the short term forecasting. NWP models have ability to resolve the wind turbine drag and turbulent mixing of upstream wind farm and can evaluate the irregularities by the wake without using extensive computational power, unlike LES [11].

Summary

Around the globe, many methods of forecasting have been done by using different techniques. The forecasting involves the prediction of wind resources for the sites and wind power plants. Statistical and Physical methods are the two types commonly used for forecasting. The WRF mesoscale model can be used for the wind speed and power forecasting of the wind farm and can be used to estimate the wind wakes using wind farm parameterization schemes.

References

- [1] A. R. Daniel and A. A. Chen, “Stochastic simulation and forecasting of hourly average wind speed sequences in Jamaica,” *Sol. Energy*, vol. 46, no. 1, pp. 1–11, 1991.
- [2] A. J. Deppe, W. A. Gallus, and E. S. Takle, “A WRF ensemble for improved wind speed forecasts at turbine height,” *Weather Forecast.*, vol. 28, no. 1, pp. 212–228, 2013.
- [3] M. Bilal, K. Solbakken, and Y. Birkelund, “Wind speed and direction predictions by WRF and WindSim coupling over Nygårdsfjell,” *J. Phys. Conf. Ser.*, vol. 753, no. 8, 2016.
- [4] B. Efe *et al.*, “72hr forecast of wind power in Manisa, Turkey by using the WRF model coupled to WindSim,” *2012 Int. Conf. Renew. Energy Res. Appl. ICRERA 2012*, pp. 1–6, 2012.
- [5] Y. Che, X. Peng, L. Delle Monache, T. Kawaguchi, and F. Xiao, “A wind power forecasting system based on the weather research and forecasting model and Kalman filtering over a wind-farm in Japan,” *J. Renew. Sustain. Energy*, vol. 8, no. 1, 2016.
- [6] G. Martínez-Arellano and L. Nolle, “Short-term wind power forecasting with WRF-ARW model and genetic programming,” *Mendel*, pp. 51–56, 2013.
- [7] M. F. Howland, S. K. Lele, and J. O. Dabiri, “Wind farm power optimization through wake steering,” *Proc. Natl. Acad. Sci.*, vol. 116, no. 29, pp. 14495–14500, 2019.
- [8] J. Schmidt and B. Stoevesandt, “The impact of wake models on wind farm layout optimization,” *J. Phys. Conf. Ser.*, vol. 625, no. 1, 2015.
- [9] N. G. Nygaard and S. D. Hansen, “Wake effects between two neighbouring wind farms,” *J. Phys. Conf. Ser.*, vol. 753, no. 3, 2016.
- [10] A. Keane, P. E. O. Aguirre, H. Ferchland, P. Clive, and D. Gallacher, “An analytical

- model for a full wind turbine wake,” *J. Phys. Conf. Ser.*, vol. 753, no. 3, 2016.
- [11] J. K. Lundquist, K. K. DuVivier, D. Kaffine, and J. M. Tomaszewski, “Costs and consequences of wind turbine wake effects arising from uncoordinated wind energy development,” *Nat. Energy*, vol. 4, no. 1, pp. 26–34, 2019.
- [12] F. González-Longatt, P. P. Wall, and V. Terzija, “Wake effect in wind farm performance: Steady-state and dynamic behavior,” *Renew. Energy*, vol. 39, no. 1, pp. 329–338, 2012.
- [13] D. C. Li, C. J. Chang, C. C. Chen, and W. C. Chen, “Forecasting short-term electricity consumption using the adaptive grey-based approach-An Asian case,” *Omega*, vol. 40, no. 6, pp. 767–773, 2012.
- [14] M. A. Prósper, C. Otero-Casal, F. C. Fernández, and G. Miguez-Macho, “Wind power forecasting for a real onshore wind farm on complex terrain using WRF high resolution simulations,” *Renew. Energy*, vol. 135, pp. 674–686, 2019.
- [15] L. Li, Y. M. Wang, and Y. Q. Liu, “Impact of wake effect on wind power prediction,” *IET Conf. Publ.*, vol. 2013, no. 623 CP, pp. 20–23, 2013.
- [16] S. S. Soman, H. Zareipour, O. Malik, and P. Mandal, “A review of wind power and wind speed forecasting methods with different time horizons,” *North Am. Power Symp. 2010, NAPS 2010*, 2010.
- [17] E. A. Bossanyi, “Short-Term Wind Prediction Using Kalman Filters,” *Wind Eng.*, vol. 9, no. 1, pp. 1–8, 1985.
- [18] A. Sfetsos, “A novel approach for the forecasting of mean hourly wind speed time series,” *Renew. Energy*, vol. 27, no. 2, pp. 163–174, 2002.
- [19] M. Mohandes, S. Rehman, and T. O. Halawani, “Estimation of global solar radiation using artificial neural networks,” *Renew. Energy*, vol. 14, no. 1–4, pp. 179–184, 1998.
- [20] A. Alexandridis and A. Zapranis, “Wind Derivatives: Modeling and Pricing,” *Comput. Econ.*, vol. 41, no. 3, pp. 299–326, 2013.

- [21] M. Monfared, S. K. Y. Nikraves, and H. Rastegar, "A Novel Fuzzy Predictor for Wind Speed," *Lect. Notes Eng. Comput. Sci.*, vol. 2167, no. 1, pp. 840–843, 2007.
- [22] profil kesehatan indonesia, "Provil Kesehatan Indonesia 2018," vol. 16, p. 496, 2018.
- [23] P. P. Craig, A. Gadgil, and J. G. Koomey, "What Can History Teach Us? A Retrospective Examination of Long-Term Energy Forecasts for the United States," *Annu. Rev. Energy Environ.*, vol. 27, no. 1, pp. 83–118, 2002.
- [24] G. Giebel and L. Landberg, "State-of-the-Art on Methods and Software Tools for Short-Term Prediction of Wind Energy Production," *Energy*, pp. 16–19, 2010.
- [25] C. W. Potter and M. Negnevitsky, "Very short-term wind forecasting for Tasmanian power generation," *IEEE Trans. Power Syst.*, vol. 21, no. 2, pp. 965–972, 2006.
- [26] L. Landberg, "A mathematical look at a physical power prediction model," *Wind Energy*, vol. 1, no. 1, pp. 23–28, 1998.
- [27] S. Al-Yahyai, Y. Charabi, and A. Gastli, "Review of the use of numerical weather prediction (NWP) models for wind energy assessment," *Renew. Sustain. Energy Rev.*, vol. 14, no. 9, pp. 3192–3198, 2010.
- [28] K. Solbakken and Y. Birkelund, "Evaluation of the Weather Research and Forecasting (WRF) model with respect to wind in complex terrain," *J. Phys. Conf. Ser.*, vol. 1102, no. 1, 2018.
- [29] W.-Y. Chang, "A Literature Review of Wind Forecasting Methods," *J. Power Energy Eng.*, vol. 02, no. 04, pp. 161–168, 2014.
- [30] W. C. Skamarock *et al.*, "A Description of the Advanced Research WRF Model Version 4 NCAR Technical Note," *Natl. Cent. Atmos. Res.*, p. 145, 2019.
- [31] T. Prabha and G. Hoogenboom, "Evaluation of the Weather Research and Forecasting model for two frost events," *Comput. Electron. Agric.*, vol. 64, no. 2, pp. 234–247, 2008.

- [32] M. Amjad, Q. Zafar, F. Khan, and M. M. Sheikh, "Evaluation of weather research and forecasting model for the assessment of wind resource over Ghara, Pakistan," *Int. J. Climatol.*, vol. 35, no. 8, pp. 1821–1832, 2015.
- [33] J. G. Powers *et al.*, "The weather research and forecasting model: Overview, system efforts, and future directions," *Bull. Am. Meteorol. Soc.*, vol. 98, no. 8, pp. 1717–1737, 2017.
- [34] Pedro A. Jimenez, "10 jamCd120266 1610..1617.pdf." .
- [35] D. Carvalho, A. Rocha, C. S. Santos, and R. Pereira, "Wind resource modelling in complex terrain using different mesoscale-microscale coupling techniques," *Appl. Energy*, vol. 108, pp. 493–504, 2013.
- [36] S. Dee, J. Emile-Geay, M. N. Evans, A. Allam, E. J. Steig, and Thompson, "Journal of Advances in Modeling Earth Systems," *J. Adv. Model. Earth Syst.*, vol. 6, pp. 513–526, 2014.
- [37] J. D. Mirocha, B. Kosovic, M. L. Aitken, and J. K. Lundquist, "Implementation of a generalized actuator disk wind turbine model into the weather research and forecasting model for large-eddy simulation applications," *J. Renew. Sustain. Energy*, vol. 6, no. 1, 2014.
- [38] A. Chaudhari, A. Hellsten, and J. Hämäläinen, "Full-Scale Experimental Validation of Large-Eddy Simulation of Wind Flows over Complex Terrain: The Bolund Hill," *Adv. Meteorol.*, vol. 2016, 2016.

Chapter 3

Wind farms specification and WRF configuration

3.1 Wind Farm Parameters

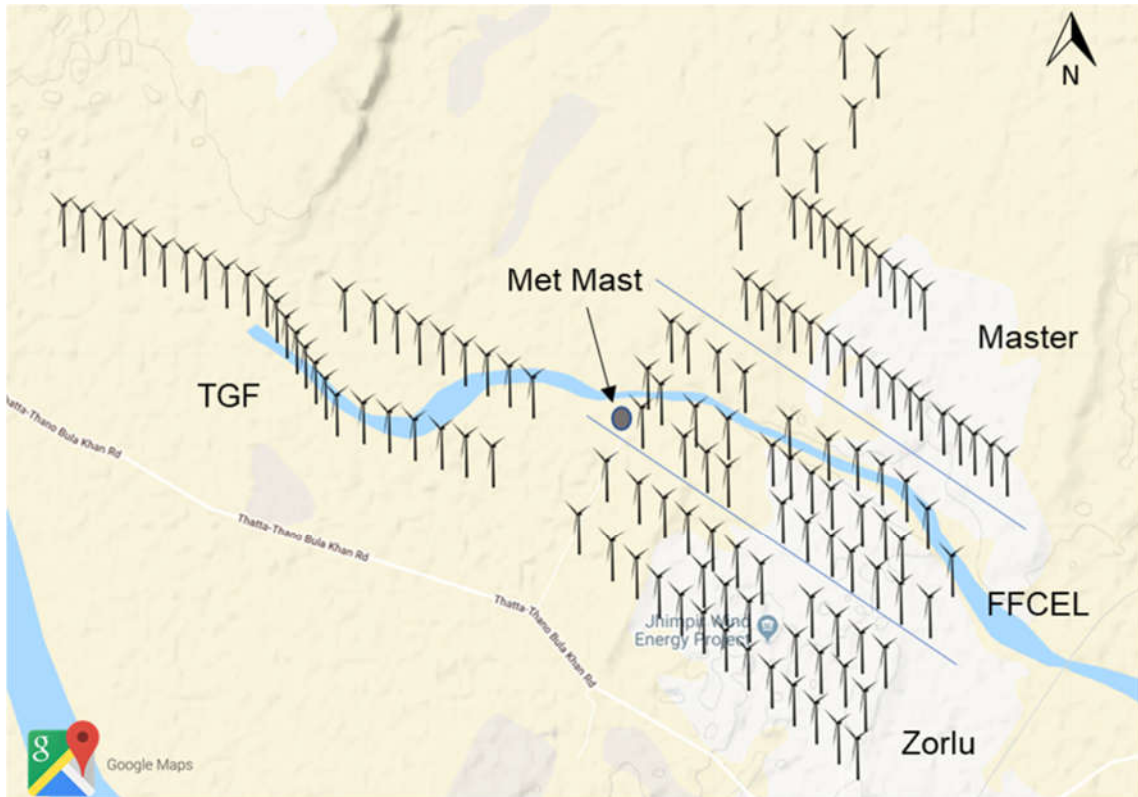


Figure 3.1 Layout of the FFCEL wind farm with neighboring wind farm

FFC Energy Limited (FFCEL) is in the Jhimpir wind corridor, which is in the southern province of Pakistan. It is operational since 2013. It has a production capacity of 49.5 MW. It contains 33 S77 Nordex wind turbines, each having a maximum power of 1500 KW. The hub height and rotor diameter of the wind turbines are 80 m and 77 m, respectively. The topography of the area where the farm is situated is complex. The FFCEL wind farm is surrounded by three neighboring wind farms operated by Zorlu in the south-west, Three Gorges First (TGF) in the north-west, and Master Wind Energy

limited (MWEL) in the north-east side is shown in Figure 3.1. The technical details of the four wind farms are shown in Table 3.1

Table 3.1 Wind Farm specification of the FFCEL with neighboring wind

| Wind Farm | FFCEL | Zorlu | | TGF | Master |
|-------------------------------------|-------------|-------------------|------------------|----------------------|-------------|
| Wind Turbine Model | Nordex S77 | Vestas V90 1.8 MW | VensysV62 1.2 MW | Goldwind GW77 1.5 MW | GE 1.6 XLE |
| No. of Wind Turbines | 33 x 1.5 MW | 28 x 1.8 MW | 5 x 1.2 MW | 33 x 1.5 MW | 33 x 1.6 MW |
| Rotor diameter (m) | 77 | 90 | 62 | 77 | 82.5 |
| Hub Height (m) | 80 | 80 | 69 | 85 | 80 |
| Power Density (m ² / kW) | 3.11 | 3.5 | 2.5 | 3.1 | 3.6 |
| Distance from the FFCEL (m) | - | ~790 | | ~1390 | ~800 |

3.2 WRF Model Configuration

The WRF version 4.1 is used for the study, which is the latest version used for operational weather forecasting and atmospheric research [1]. The resolution of spatial grids can be increased up to a few hundred meters in the WRF. The model is set up for four two-way nested domains with an advanced horizontal resolution of 9000, 3000, 1000, and 333.33m. Warner's [2] requirement for setting up the domains was fulfilled including the parent (d01) and three nested grids (d02, d03, d04). Domain and grids point resolution is shown in Table 3-2. The innermost domain d04 is centered at 25.075 °N and 67.972 °E, which is the location of a met mast located adjacent to the FFCEL wind farm. The highest resolution domain covers an approximate area of 55 km x 55 km, which gives suitable information about the meteorological effects which are occurring locally near the wind farm. The 333m innermost domain's resolution gives more than adequate information regarding the wind farm and topographical characteristics of terrain [3]-[4]. This scheme represents the turbine as a source of turbulence that converts the kinetic energy into useful energy (extracted by the turbine) and turbulent kinetic energy in the form of wind turbine wake to the downstream wakes.

Table 3.2 Detail of domains and grid points

| Domains | 1 | 2 | 3 | 4 |
|-----------------|----------|-----------|-----------|-----------|
| Grid Points | 79 x 79 | 112 x 112 | 142 x 142 | 166 x 166 |
| dx=dy (km) | 9 | 3 | 1 | 0.33 |
| Vertical Levels | 40 | 40 | 40 | 40 |

Global Forecasting System (GFS) [5] data of grid-scale 004 (0.50) is used as an initial condition. The data was obtained from the National Center of Environmental Prediction

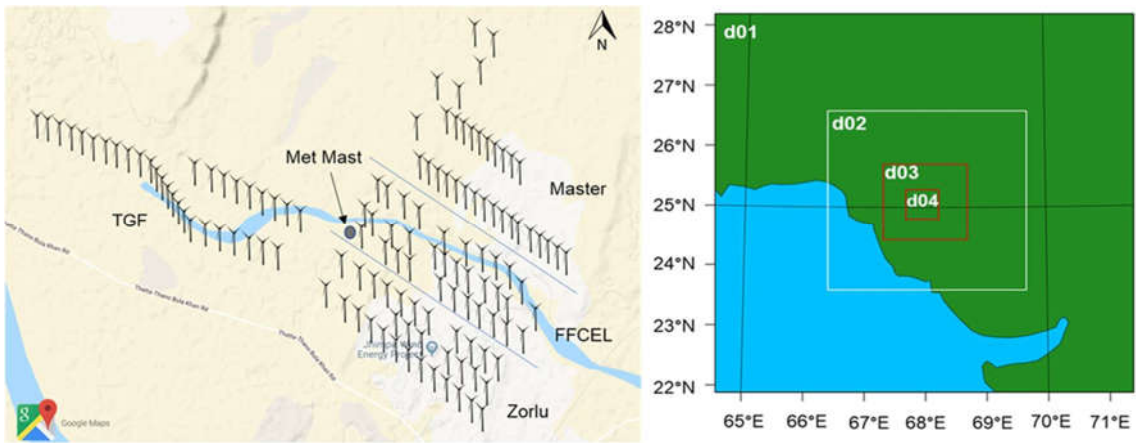


Figure 3.2 a) Wind farm layout

b) WRF model nested domains

(NCEP), which updated after 6h interval. The data is publicly available for commercial use. The Moderate Resolution Imaging Spectroradiometer (MODIS) data with a high resolution of 30 arc seconds was used as a boundary condition in the forecasting model.

The physics schemes option includes the newer version of the rapid radiative transfer model for both long and short wave [6]. New Thompson et al. [7] is used for the microphysical process. The land fluxes were resolved by the unified Noah model [8]. The turbulent phenomena near the boundary layer were resolved by the Mellor-Yamada [9] planetary boundary layer scheme. Convection which is occurring during the interaction of the atmosphere is characterized by the Tiedtke scheme [10].

The wind farm parameterization scheme which was developed by Fitch et al. [11] is used to evaluate the wind turbine wakes and effects on wind power production. This scheme represents the turbine as a source of turbulence that converts the kinetic energy into useful energy (extracted by the turbine) and turbulent kinetic energy in the form of wind turbine

wake to the downstream wakes. The vertical shear produce near the boundary layer of the surface by the momentum sink is accounted for by the MYNN. The effects of buoyancy and stability after the momentum sink and turbulent mixing is also characterized by the planetary boundary layer scheme MYNN.

3.3 Simulation Setup

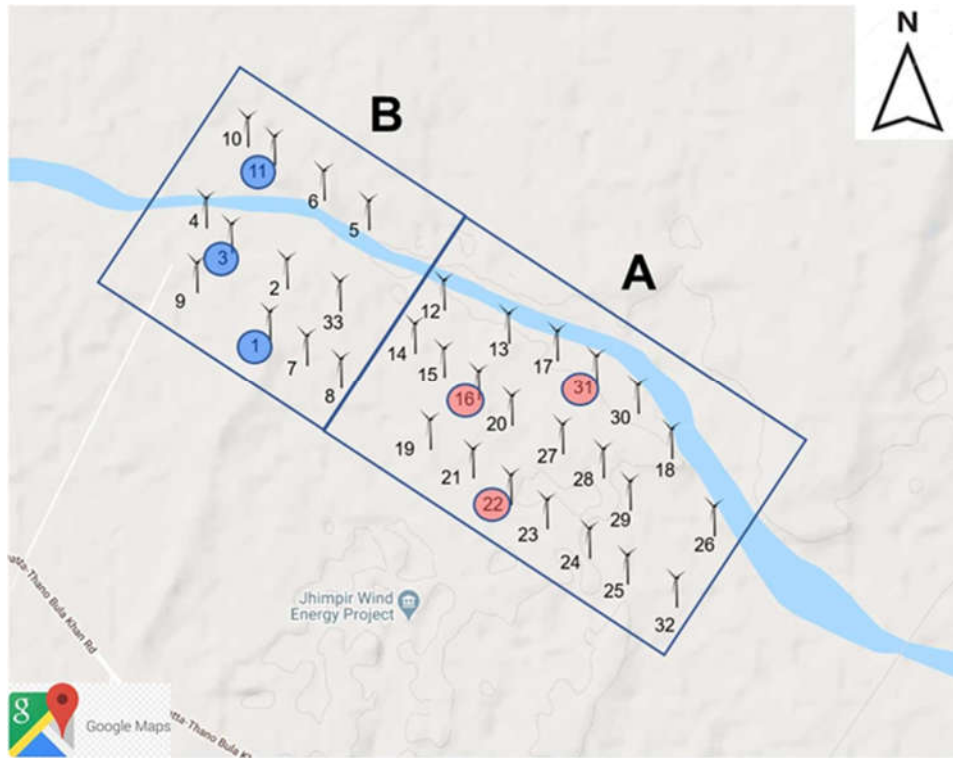


Figure 3.3 Wind farm layout, categorizing wind turbines in two sets i.e. A: with less intra-farm spacing between wind turbines, B: With more intra-farm spacing between them

Table 3.3 Simulation design for two cases i.e. Without Inter-farm and With Inter-farm wakes

| | Case 1: Without considering inter-farm wake | | Case 2: With considering inter-farm wake | |
|---------------|--|----------------------------|---|----------------------------|
| Season | Beginning Date | End Date | Beginning Date | End Date |
| Summer | 1 Jun 2018, 0000 hrs. UTC | 8 June 2018, 0000 hrs. UTC | 1 June 2018, 0000 hrs. UTC | 8 June 2018, 0000 hrs. UTC |
| | 1 Jul 2018, 0000 hrs. UTC | 8 July 2018, 0000 hrs. UTC | 1 July 2018, 0000 hrs. UTC | 8 July 2018, 0000 hrs. UTC |
| Winter | 1 Jan 2019, 0000 hrs. UTC | 8 Jan 2019, 0000 hrs. UTC | 1 Jan 2019, 0000 hrs. UTC | 8 Jan 2019, 0000 hrs. UTC |

To evaluate the influence of wind farms' wake effects on the accuracy of wind speed forecasting, two different sets of simulations were designed. One set included the inter-farm wake effects emerging from the three neighboring wind farms, while the other set catered only the intra-farm wake effects of FFCEL and ignored the inter-farm wakes. Both sets were simulated for 7 days in two summer months of June and July and a winter month of January is shown in Table 3.3. The wind characteristics remarkably alter between the two seasons so the effect of seasonal variation on forecasting accuracy was essential to study. The wind speed and power results obtained from this study were also compared with the observed data obtained from the FFCEL wind farm. The forecasted wind speed at the turbine hub height is then used for power calculation using the power curve provided by the manufacturer of the wind turbine.

Summary

The FFCEL wind farm has the capacity of a power generation of 49.5 MW. It is surrounded by three neighboring wind farms. The WRF is used for the wind resource prediction of the FFCEL wind farm. Different physics schemes have been used to simplify the atmospheric interaction with the terrain. Simulations were designed to cater to the effect of wakes of neighboring wind farms in two different seasons of years.

References

- [1] W. C. Skamarock *et al.*, “A Description of the Advanced Research WRF Model Version 4 NCAR Technical Note,” *Natl. Cent. Atmos. Res.*, p. 145, 2019.
- [2] T. T. Warner, “Quality assurance in atmospheric modeling,” *Bull. Am. Meteorol. Soc.*, vol. 92, no. 12, pp. 1601–1610, 2011.
- [3] M. A. Prósper, C. Otero-Casal, F. C. Fernández, and G. Miguez-Macho, “Wind power forecasting for a real onshore wind farm on complex terrain using WRF high resolution simulations,” *Renew. Energy*, vol. 135, pp. 674–686, 2019.
- [4] Pedro A. Jimenez, “10 jamCd120266 1610..1617.pdf.” .
- [5] A. Jabbari, J.-M. So, and D.-H. Bae, “Accuracy assessment of real-time flood forecasting of coupled hydrological and mesoscale meteorological models,” *Nat. Hazards Earth Syst. Sci. Discuss.*, no. January, pp. 1–36, 2018.
- [6] M. J. Iacono, J. S. Delamere, E. J. Mlawer, M. W. Shephard, S. A. Clough, and W. D. Collins, “Radiative forcing by long-lived greenhouse gases: Calculations with the AER radiative transfer models,” *J. Geophys. Res. Atmos.*, vol. 113, no. D13, 2008.
- [7] G. Thompson, P. R. Field, R. M. Rasmussen, and W. D. Hall, “Explicit Forecasts of Winter Precipitation Using an Improved Bulk Microphysics Scheme. Part II: Implementation of a New Snow Parameterization,” *Mon. Weather Rev.*, vol. 136, no. 12, pp. 5095–5115, 2008.
- [8] Z.-L. Yang *et al.*, “The community Noah land surface model with multiparameterization options (Noah-MP): 2. Evaluation over global river basins,” *J. Geophys. Res. Atmos.*, vol. 116, no. D12, Jun. 2011.
- [9] M. NAKANISHI and H. NIINO, “Development of an Improved Turbulence Closure Model for the Atmospheric Boundary Layer,” *J. Meteorol. Soc. Japan. Ser. II*, vol. 87, no. 5, pp. 895–912, 2009.
- [10] C. Zhang, Y. Wang, and K. Hamilton, “Improved Representation of Boundary

Layer Clouds over the Southeast Pacific in ARW-WRF Using a Modified Tiedtke Cumulus Parameterization Scheme,” *Mon. Weather Rev.*, vol. 139, no. 11, pp. 3489–3513, 2011.

- [11] A. C. Fitch *et al.*, “Local and Mesoscale Impacts of Wind Farms as Parameterized in a Mesoscale NWP Model,” *Mon. Weather Rev.*, vol. 140, no. 9, pp. 3017–3038, Mar. 2012.

Chapter 4

WRF Model Validation

4.1 Error Parameters

The real-time observed data from the met mast and wind speed and power data from the wind turbine are utilized to assess the accuracy of forecasting skills of the WRF forecasting model. Wind speed data from the turbine was collected by the anemometer located on the nacelle of each turbine. The data was available for the 10 min interval frequency, where each point represents the average of 10 mins. The data collected from the nacelle give the real scenario on the turbine height [1].

Different statistical parameters are then computed to analyze the ability of forecasted accuracy of the model. Mean absolute error (MAE) is the most important, is used to check the precision of the model. It represents the absolute average error between forecasted and observed values. To check, whether the model is overestimating or underestimating the forecasted values from the observed values, there is another parameter, mean bias error (MBE), which gives adequate information about the sensitivity of the model. Root mean square error (RMSE) is a measure of the absolute deviation of forecasted values from the observed values. With respect to power prediction, normalized mean absolute error (NMAE) is used, it represents the normalized mean absolute error of power prediction in each turbine. In Equations 1-4 [2] i represent the observation in time, n is the total number of observations, f and Obs are predicted and observed values, respectively

$$MAE = \frac{1}{n} \sum_{i=1}^n |Obs_i - f_i| \quad (1)$$

$$MBE = \frac{1}{n} \sum_{i=1}^n (Obs_i - f_i) \quad (2)$$

$$RMSE = \sqrt{\frac{\sum_{i=1}^n (Obs_i - f_i)^2}{n}} \quad (3)$$

$$NMAE = \frac{\frac{1}{n} \sum_{i=1}^n |Obs_i - f_i|}{NP} \quad (4)$$

The wind direction is also an important parameter to check the forecasted skills of the model. Wind direction predicted by the WRF is then compared from observed wind direction from met mast.

Table 4.1 Statistical Error analysis for both cases

| | | Case 1: Without considering inter-farm wake | | | Case 2: With considering inter-farm wake | | |
|--------|---------|--|-------------------------|--------------------------|---|-------------------------|--------------------------|
| | | MAE (ms ⁻¹) | MBE (ms ⁻¹) | RMSE (ms ⁻¹) | MAE (ms ⁻¹) | MBE (ms ⁻¹) | RMSE (ms ⁻¹) |
| Summer | June | 1.30 | -0.85 | 1.63 | 1.20 | -0.51 | 1.52 |
| | July | 1.34 | -0.57 | 1.66 | 1.32 | -0.18 | 1.64 |
| Winter | January | 1.87 | -0.15 | 2.42 | 1.59 | 0.25 | 2.02 |

Table 4.1 represents the error in both cases as the WRF predicted the wind speed during the simulation.

Summary

Different statistical error assessment was performed to assess the forecasting skills of the WRF mesoscale forecasting model. The output of the WRF models was compared with the observed data of the met mast and wind farm. A considerable amount of error reduction was observed for Case 2 when inter-farm was included in wind resource forecasting.

References

- [1] Y. Che, X. Peng, L. Delle Monache, T. Kawaguchi, and F. Xiao, “A wind power forecasting system based on the weather research and forecasting model and Kalman filtering over a wind-farm in Japan,” *J. Renew. Sustain. Energy*, vol. 8, no. 1, 2016.
- [2] M. A. Prósper, C. Otero-Casal, F. C. Fernández, and G. Miguez-Macho, “Wind power forecasting for a real onshore wind farm on complex terrain using WRF high resolution simulations,” *Renew. Energy*, vol. 135, pp. 674–686, 2019.

Chapter 5

Results and Discussion

5.1 Wind speed and Direction analysis

Wind speed from both cases i.e. Case 1: without inter-farm wakes and Case 2: with inter-farm wakes were compared with met mast observed data, which is situated adjacent to the

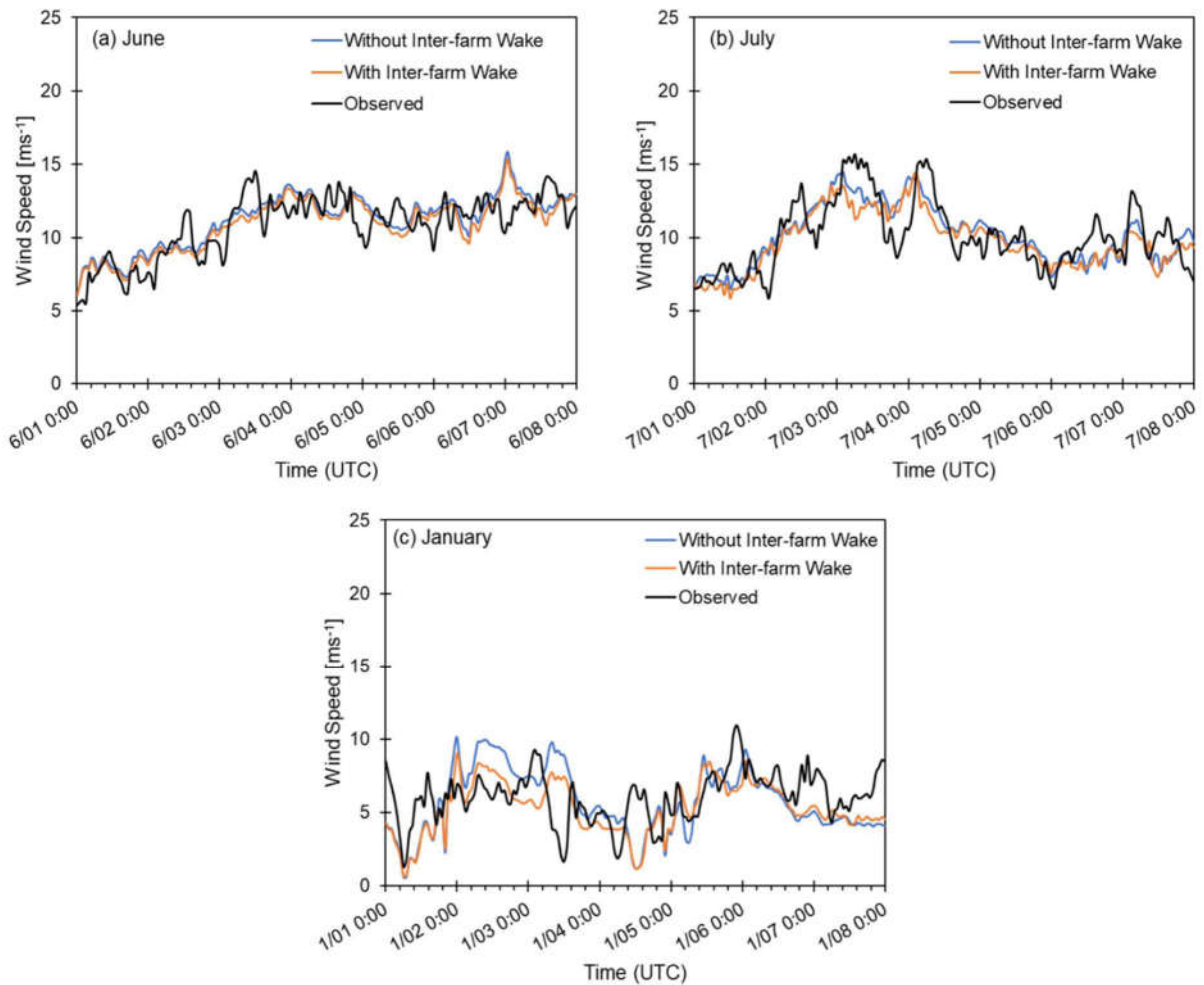


Figure 5.1 Temporal variation between forecasted (without and with inter-farm wake effects) and observed wind speed for the first week in months of (a) June, (b) July, and (c) January

FFCEL wind farm. Wind speed variation for the first seven days in June 2018, July 2018, and January 2019 is presented in Fig 5.1, where the trends for both Case 1 and Case 2 follow the observed values.

The error analysis of wind speed in the region is represented in table 4.1. A notable decrease in all the parameters was observed in Case 2 due to inter-farm wake effects. MAE was reduced to about 7.7 % for Case 2, in June in Fig 5.1. A significant improvement of

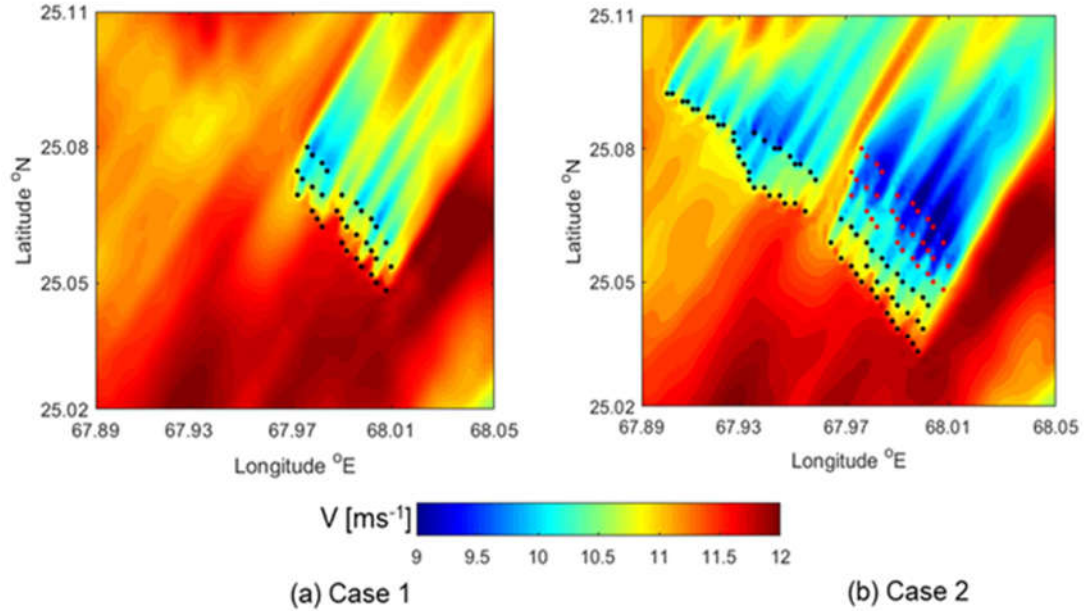


Figure 5.2 Speed deficit is observed due to the Inter farm wakes for both cases, Case 1: without Inter-farm wakes, Case 2: With inter-farm wakes, Approx. 1 ms⁻¹ of wind speed deficit is observed due to upstream wind farm

40 % was observed in MBE, for Case 1 its value is -0.85 ms⁻¹ and for Case 2 its value is -0.51 ms⁻¹. RMSE values showed a slight improvement in both cases, for Case 1 its value is 1.63 ms⁻¹ and for Case 2 its value is 1.52 ms⁻¹. For July, both cases showed mixed results with slight variations. Insignificant variation was observed for MAE and RMSE from observed values. But a considerable improvement of 68% was observed for the MBE in Case 2. Overall, the WRF model follows the observed trend with great accuracy. During January, the mean wind speeds were on the lower side than the months in summer. The RMSE and MAE are on the higher side than from summer are shown in Fig 5.1., but the reduction in the error showed the inclusion of inter-farm wake effects. 14 % MAE was improved in the Case 2 relative to Case 1, while MBE increases for Case 2 as the WRF overestimates the wakes mixing. The mean value of wind direction predicted by the WRF for the June is 222⁰, and while mean observed value of direction is 247⁰ The WRF predicted wind direction is particularly in the north west direction.

For the winter seasons, as the lead time increases the forecasting skill of model degrade

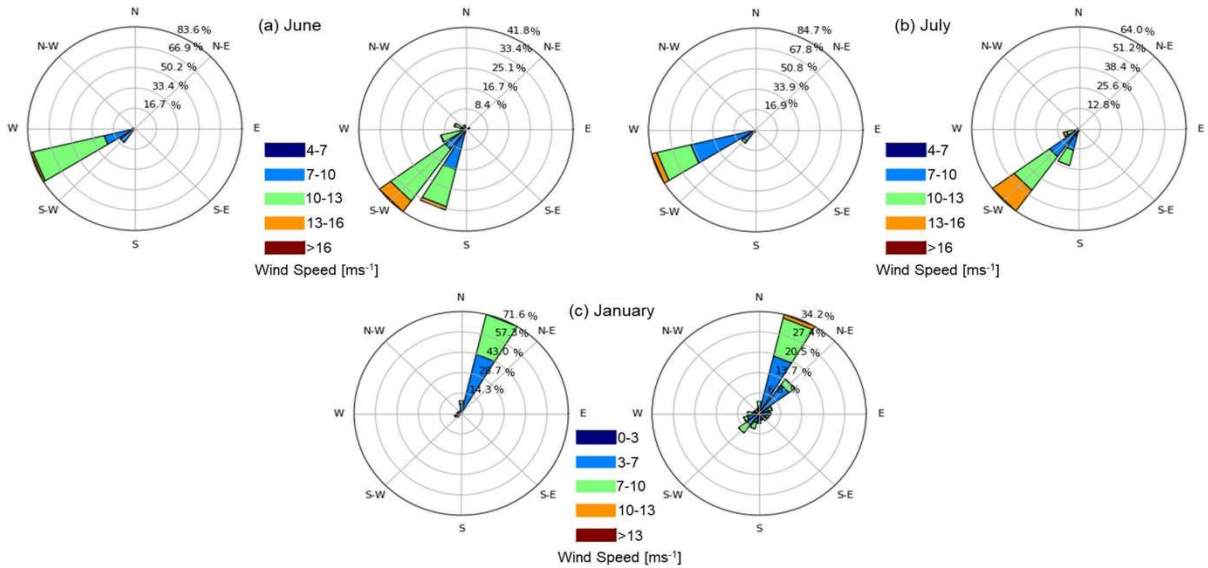


Figure 5.3 Comparison of predicted wind direction with observed values for the months of (a) June, (b) July, and (c) January

significantly. Negative MBE for almost all turbines shows that underestimation of wakes by the WRF and overestimation of speed in the summer and vice versa in the winter season. Another crucial parameter to assess the forecasting accuracy of the model is wind direction estimation. The WRF predicted wind direction for both cases with excellent similitude with the observed value of met mast, Fig 5.2. represents the wind direction in terms of wind-rose. Wind direction for Case 2 and observed

The mean value of wind direction predicted by the WRF for the June is 222° , and while mean observed value of direction is 247° . The mean difference of 33° was observed in June. For July, the mean value of direction predicted by the WRF is 224° and the observed value is 241° , the mean difference of 18° was observed. For January, the WRF predicted wind direction to be 105° , while the observed value is 80° . WRF and overestimation of speed in the summer and vice versa in the winter season. Another crucial parameter to assess the forecasting accuracy of the model is wind direction estimation WRF and overestimation of speed in the summer and vice versa in the winter season. Another crucial parameter to assess the forecasting accuracy of the model is wind direction estimation. Another crucial parameter to assess the forecasting accuracy of the model is wind direction estimation.

5.2 Error Analysis of turbines

5.2.1 Mean Absolute Error

MAE for all 33 turbines in FFCEL wind farm is determined for both cases i.e. without inter-farm wake and with inter-farm wake as shown in Fig 5-3. MAE is relatively constant throughout the summer season, with a value of around 1.23 ms^{-1} for Case 1 and 1.09 ms^{-1} for Case 2. The maximum reduction of 30% in MAE was observed for turbine 18 in Case 2. For July, a 39 % reduction in error was observed for turbine 10 for Case 2. During the month of winter, the value of MAE for both cases is higher than the summer, with an

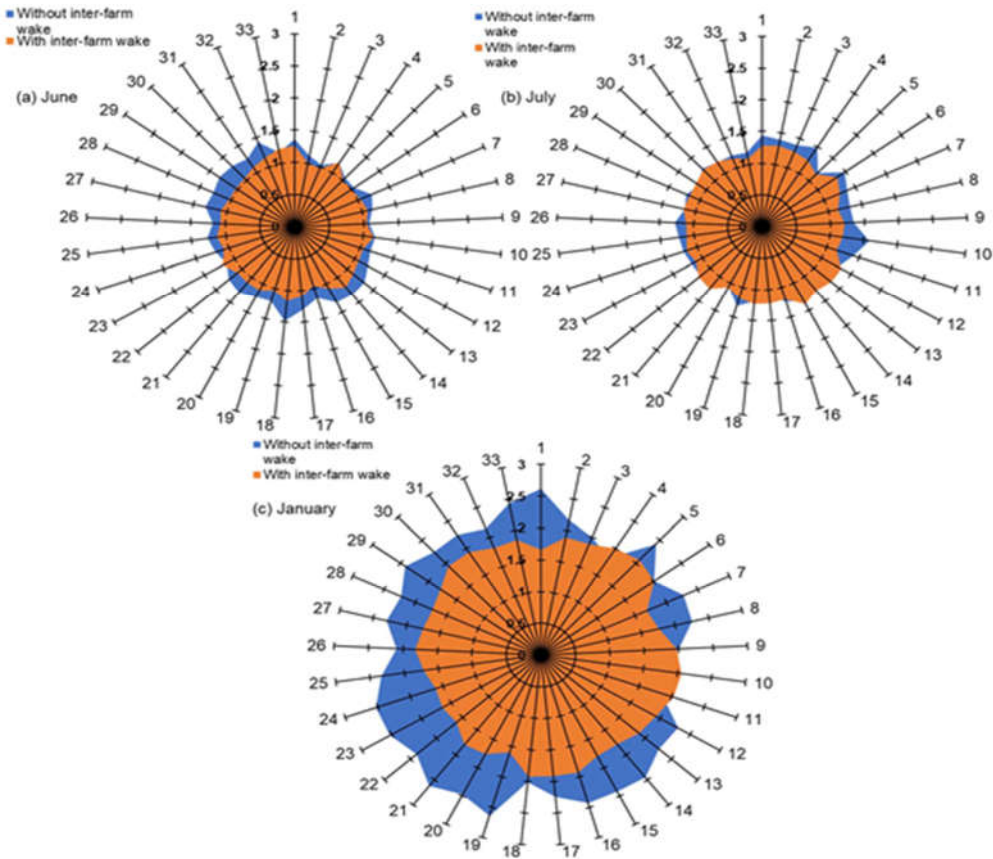


Figure 5.4 Comparison of mean absolute errors (MAE) of wind speed experienced by individual turbines for Case 1: Without inter-farm wake effects and Case 2: With inter-farm wake effects for (a) June, (b) July, and (c) January. Error values are higher in January as compared to the summer months.

average value of 2.3 ms^{-1} for Case 1 and 1.8 ms^{-1} for Case 2. The turbines 16-33 showed a significant reduction in error for Case 2. This shows that these turbines are under the influence of inter-farm wakes from upstream wind farms than the rest of the turbines.

Neglecting inter-farm wakes during the prediction of wind speed could give erroneous results.

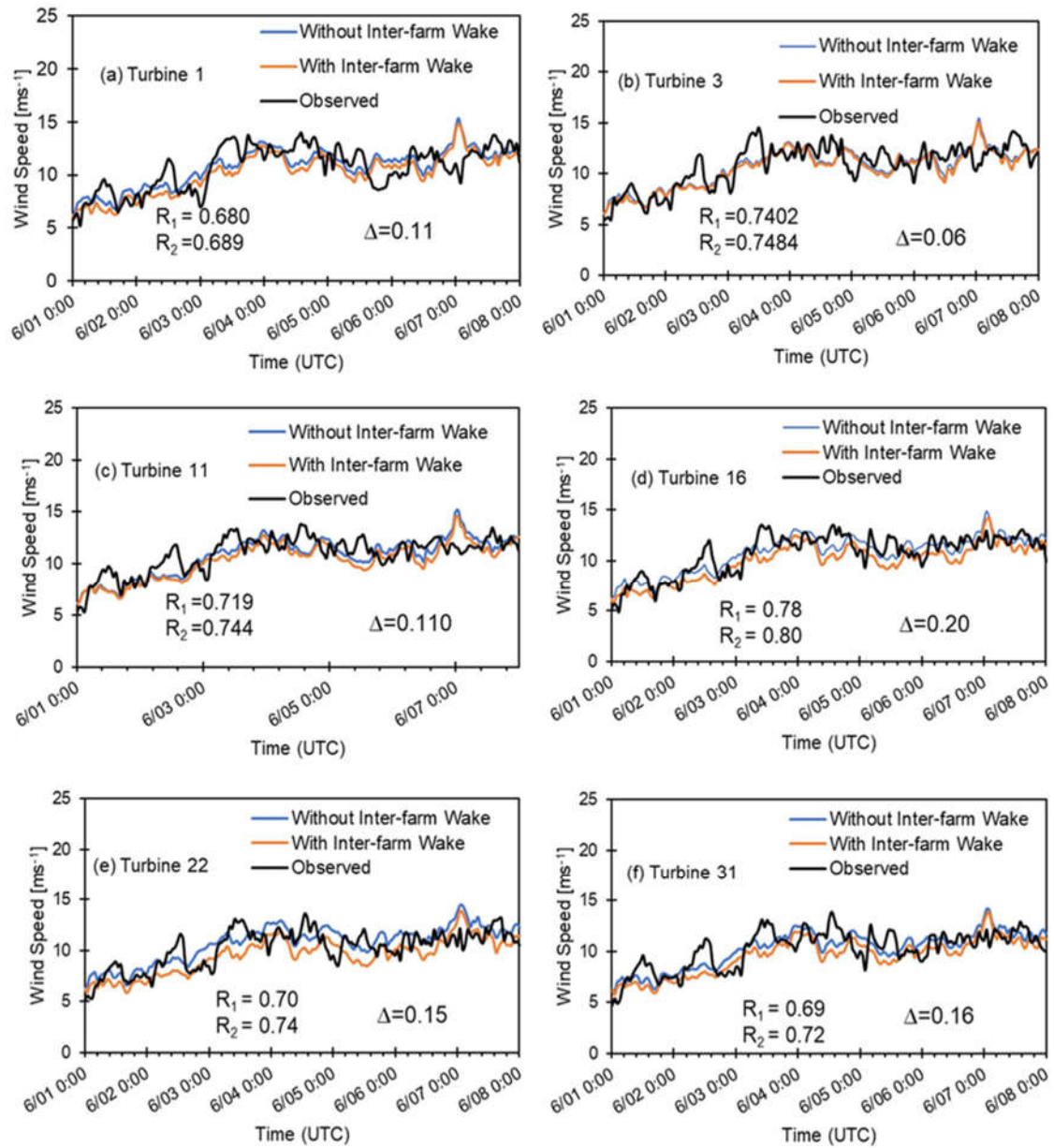


Figure 5.5 Wind speed forecasting analysis for the month of June, set A turbines are represented in (a) turbine 1, (b) Turbine 3, (c) Turbine 11, where (d) Turbine 16, (e) Turbine 22, (f) Turbine 31 represent set B turbines, Δ represents the reduced in MAE in ms^{-1} , where R_1 and R_2 represents the Pearson correlation for Case 1 and Case 2, respectively

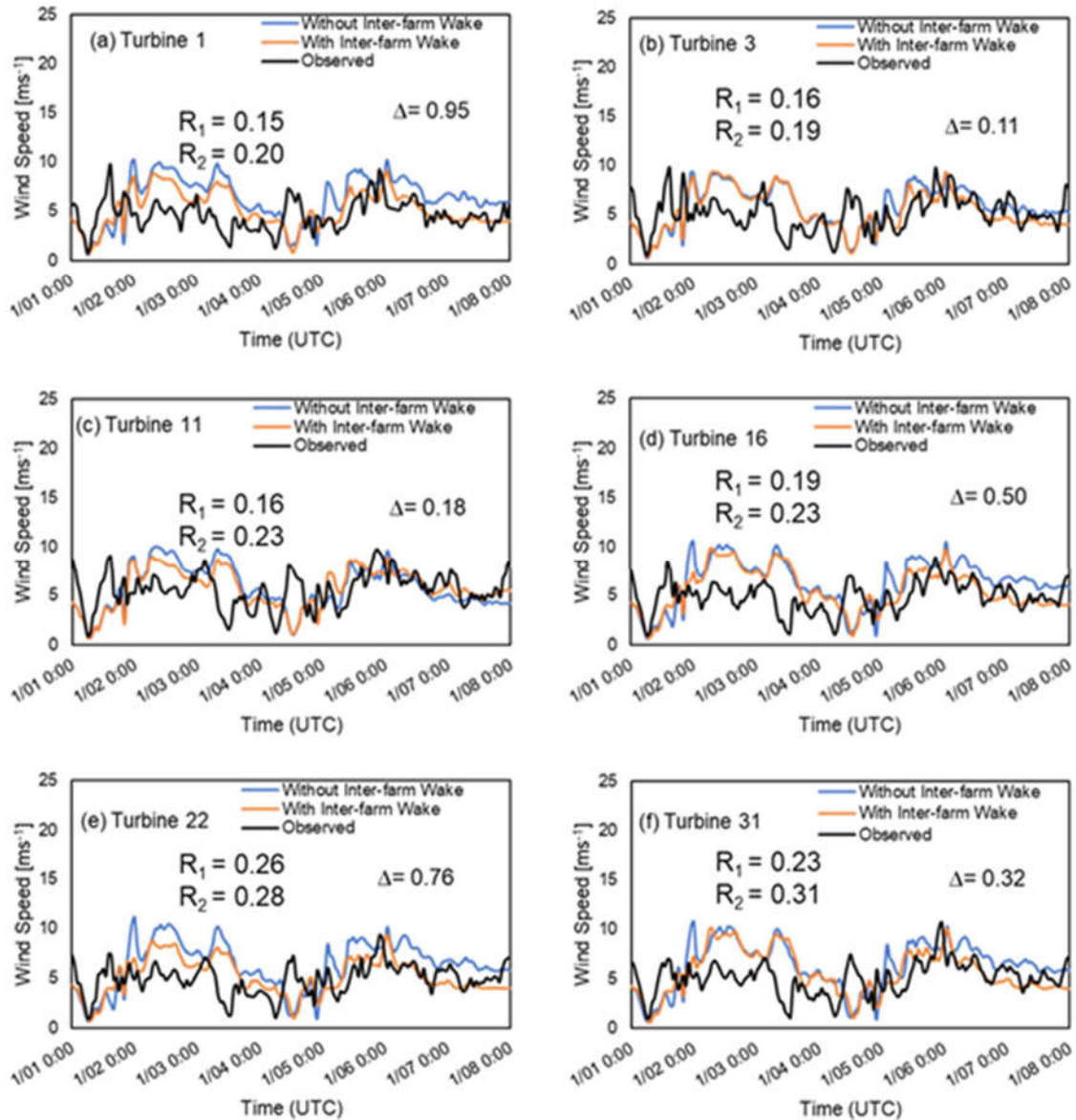


Figure 5.6 Wind speed forecasting analysis for the month of January, set A turbines is represented in (a) turbine 1, (b) Turbine 3, (c) Turbine 11, where (d) Turbine 16, (e) Turbine 22, (f) Turbine 31 represent set B turbines, Δ represents the reduction in MAE in ms^{-1} , where R_1 and R_2 represents the Pearson correlation for Case 1 and Case 2, respectively

During the first 2 days of June, the WRF showed significant error. Like wind speed, the WRF underestimated power most of the time. While in the winter, the WRF overestimates the power prediction with a larger deviation.

5.2.2 Root Mean Square Error

The RMSE is shown in the fig, for Case 1 its value is 1.53 ms^{-1} and for Case 2 it is 1.36 ms^{-1} . A maximum reduction in error of 20 % was observed in turbine 18. For July, the value of RMSE for Case 1 is 1.53 ms^{-1} and for Case 2 it is 1.36 ms^{-1} and the maximum reduction in error occurs for the turbine 10 which is 23%. Like the MAE, RMSE in the winter season is higher side than summer is shown in Fig 5.4., with the value of 2.7 ms^{-1} and 2.2 ms^{-1} for Case 1 and Case 2, respectively. During the winter month, the maximum

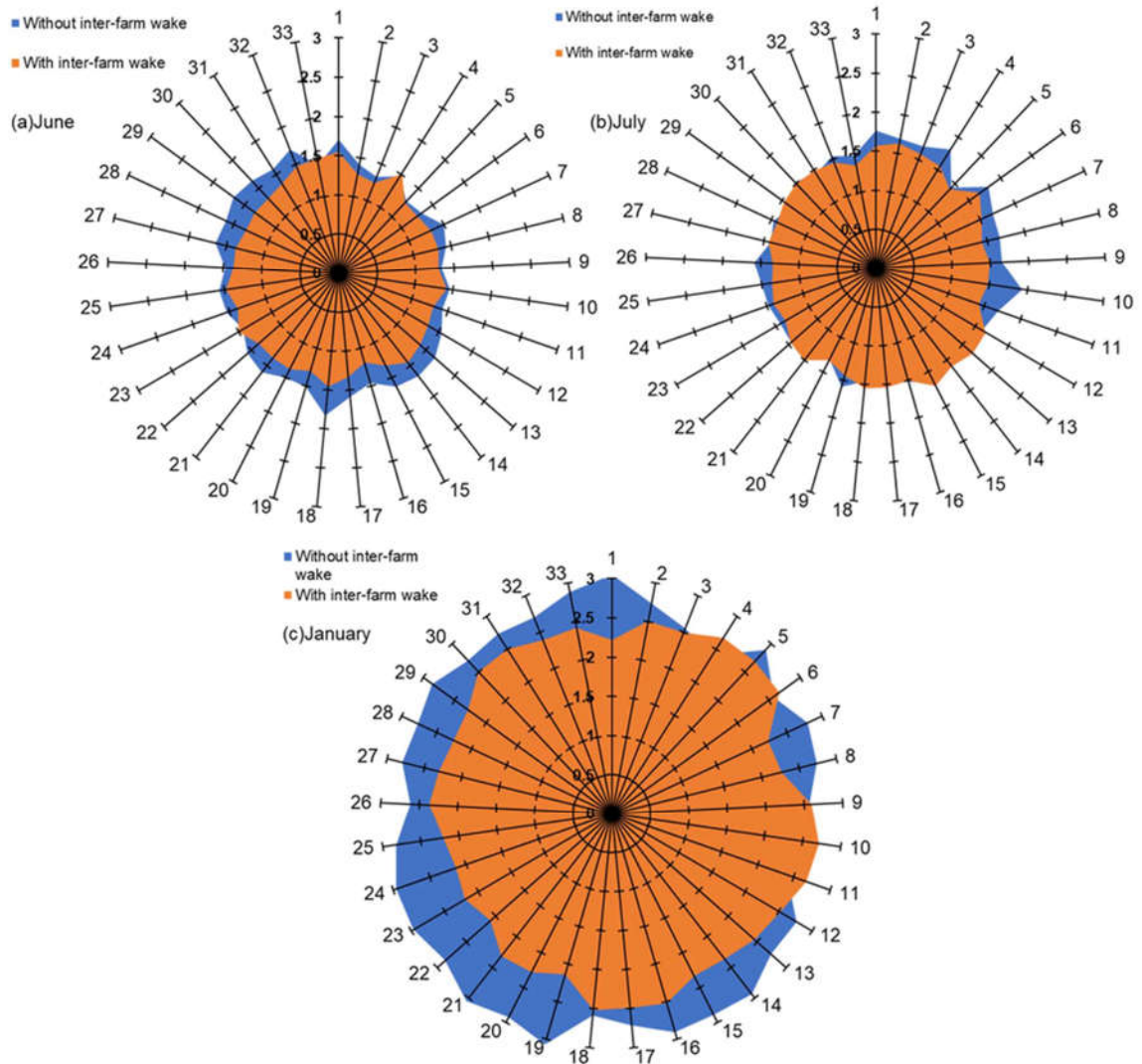


Figure 5.7 Comparison of root mean square error (RMSE) values of wind speed experienced by individual turbines for Case 1: Without inter-farm wake effects and Case 2: With inter-farm wake effects for (a) June, (b) July, and (c) January.

reduction of 30% in RMSE is observed for turbine 19.

5.3 Power Prediction Analysis

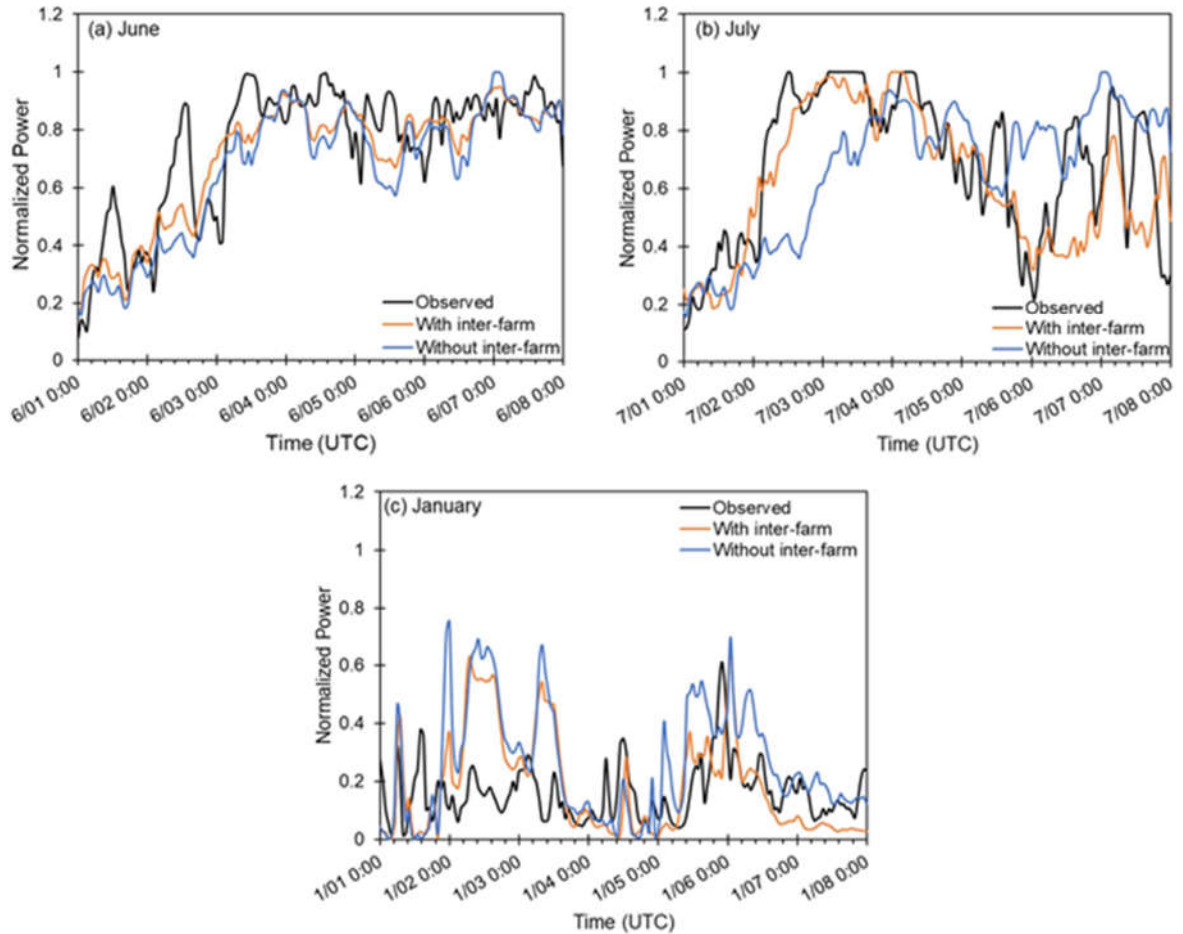


Figure 5.8 Comparison of forecasted and observed total power generation in FFCEL for Case 2: With inter-farm wake effects for the months of (a) June, (b) July, and (c) January

The total power generation of the FFCEL wind farm was predicted by the WRF for both cases and compare with the actual power production of the FFCEL in Fig 5.5., illustrates the forecasted and observed power values for seven days in June 2018, July 2018, and January 2019. During the first 2 days of June, the WRF showed significant error. Like wind speed, the WRF underestimated power most of the time. While in the winter, the WRF overestimates the power prediction with a larger deviation. The errors in wind power are higher because errors came from the wind speed prediction, small error in wind speed increased by three times for power estimation. The errors in wind power are higher because errors came from the wind speed prediction, small error in wind speed increased by three times for power estimation.

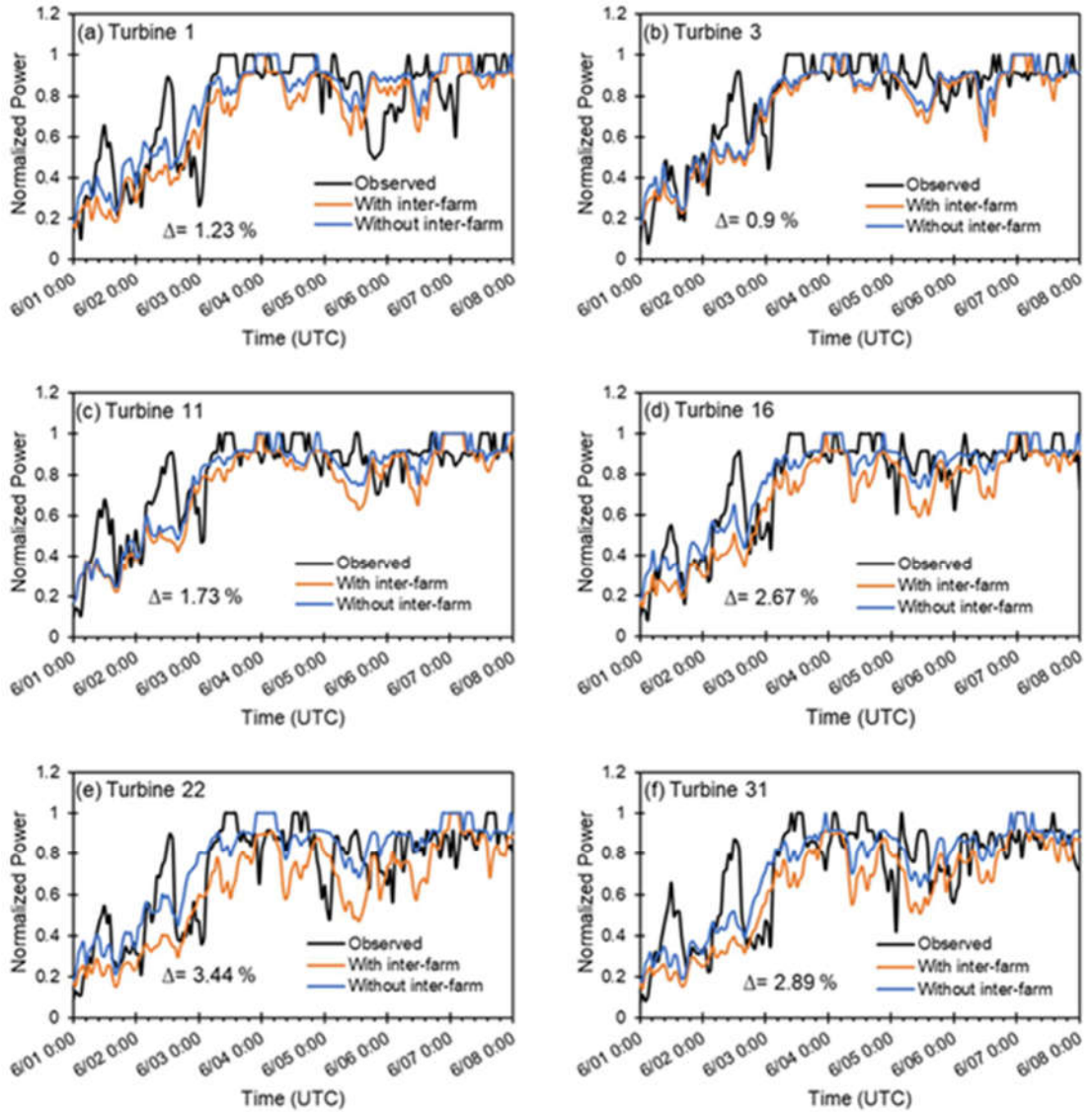


Figure 5.9 Wind power forecasting analysis for the month of June, set A turbines is represented in (a) turbine 1, (b) Turbine 3, (c) Turbine 11, where (d) Turbine 16, (e) Turbine 22, (f) Turbine 31 represent set B turbines, Δ represents the reduction in % deficit reduction in normalized power prediction

To evaluate the accuracy of the WRF in wind power prediction in determining the power output of the FFCEL, the Correlation plot is shown in Fig 5.6., For the month of June, the value of Pearson Correlation R for both cases is 0.80 and 0.82, respectively for both cases. For July, the value of R is 0.38 and 0.79, respectively for both cases. And lastly, for January, the value of R is 0.25 and 0.27, respectively. This shows that the predictive skill of the WRF is improved for Case 2 while catering to the inter-farm wake.

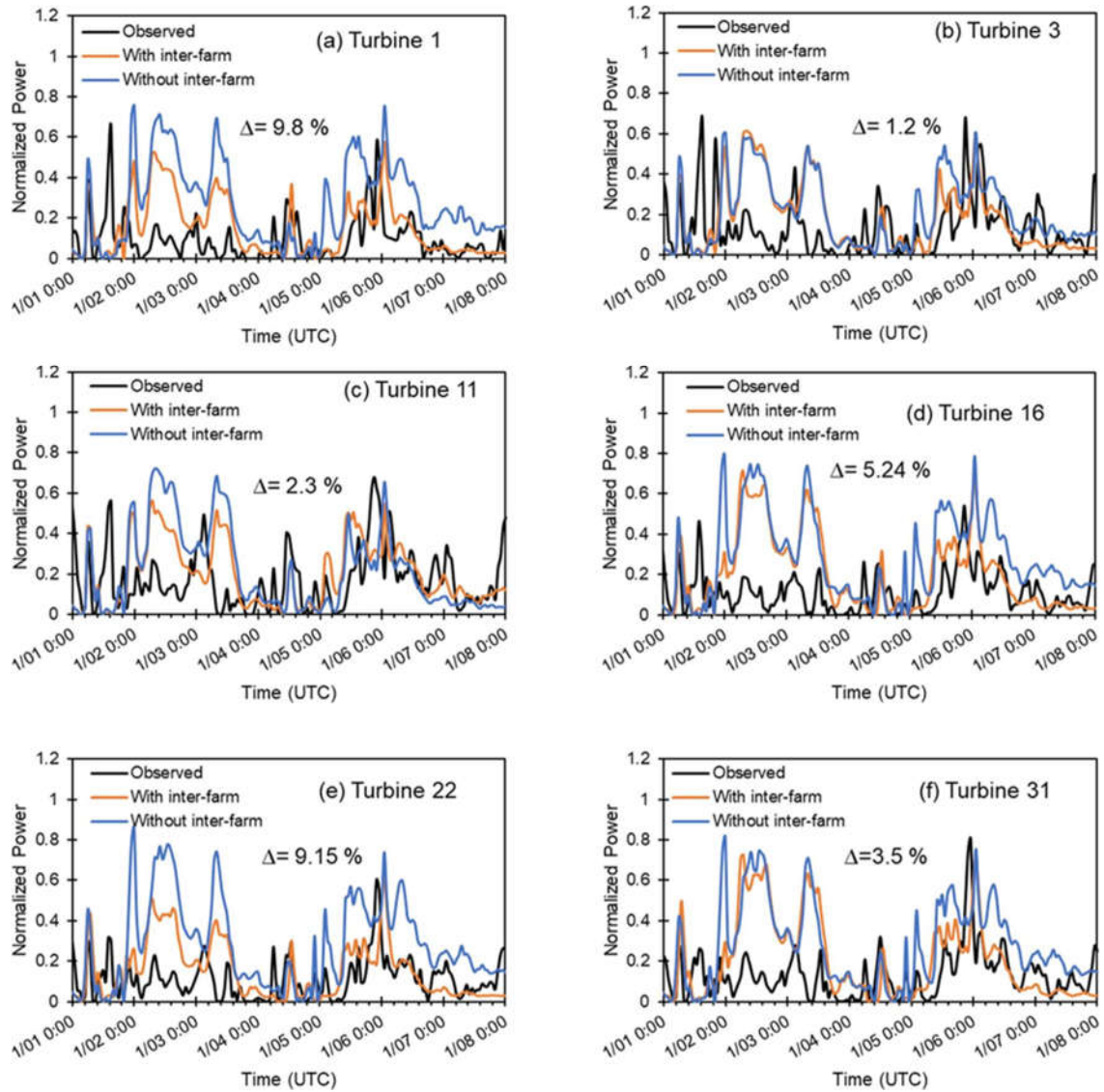


Figure 5.10 Wind power forecasting analysis for the month of January, set A turbines is represented in (a) turbine 1, (b) Turbine 3, (c) Turbine 11, where (d) Turbine 16, (e) Turbine 22, (f) Turbine 31 represent set B turbines, Δ represents the reduction in % deficit reduction in normalized power prediction

5.3.1 Normalized Mean Absolute Error

The mean value of NMAE is shown in Fig 5-7., the mean value of NMAE for all turbines in June for both cases is 13 % and 11%, respectively for Case 1 and Case 2. A maximum

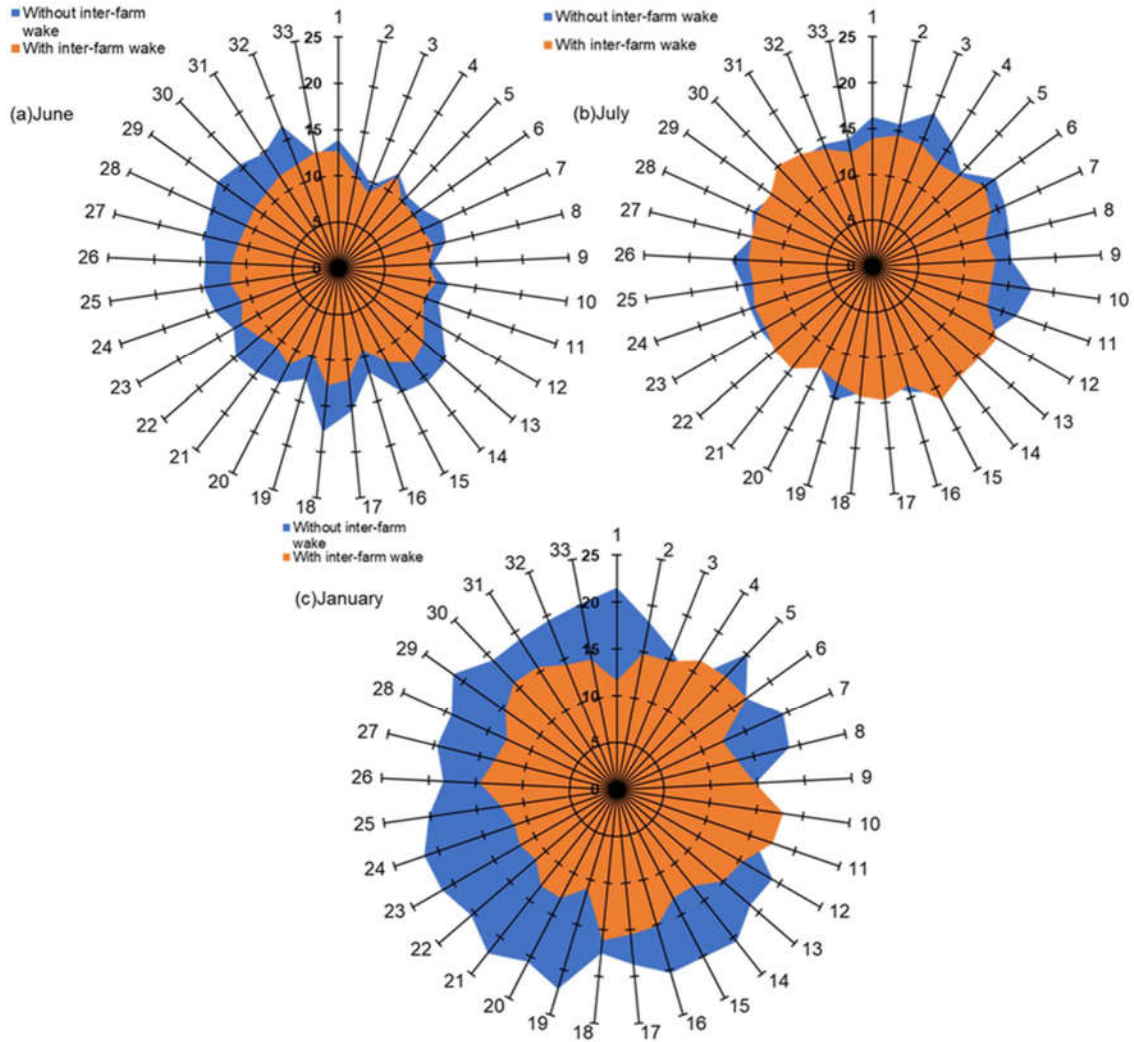


Figure 5.11 Comparison of normalized mean absolute error values, (NMAE) in %, of power generated by individual turbines for Case 1: without inter-farm wake effects and Case 2: With inter-farm wake effects

reduction of 28 % in error was observed for turbine 28. For July, the mean value of NMAE for Case 1 is 14 % and for Case 2 it is 10 %. Similar to MAE and RMSE, the value of NMAE for the winter season is on the higher side.

The mean value of NMAE for Case 1 is 19 % and Case 2 is 14 %. A maximum error reduction in prediction is observed for turbine 24, which is 47%. Another important parameter is the Pearson correlation coefficient for the normalized absolute power prediction, in June R is 0.82, while in July it is 0.79 and in January it is in the lower side, which is 0.27.

In all the parameters, catering inter-farm wakes reduced the errors and increased the forecasted skills.

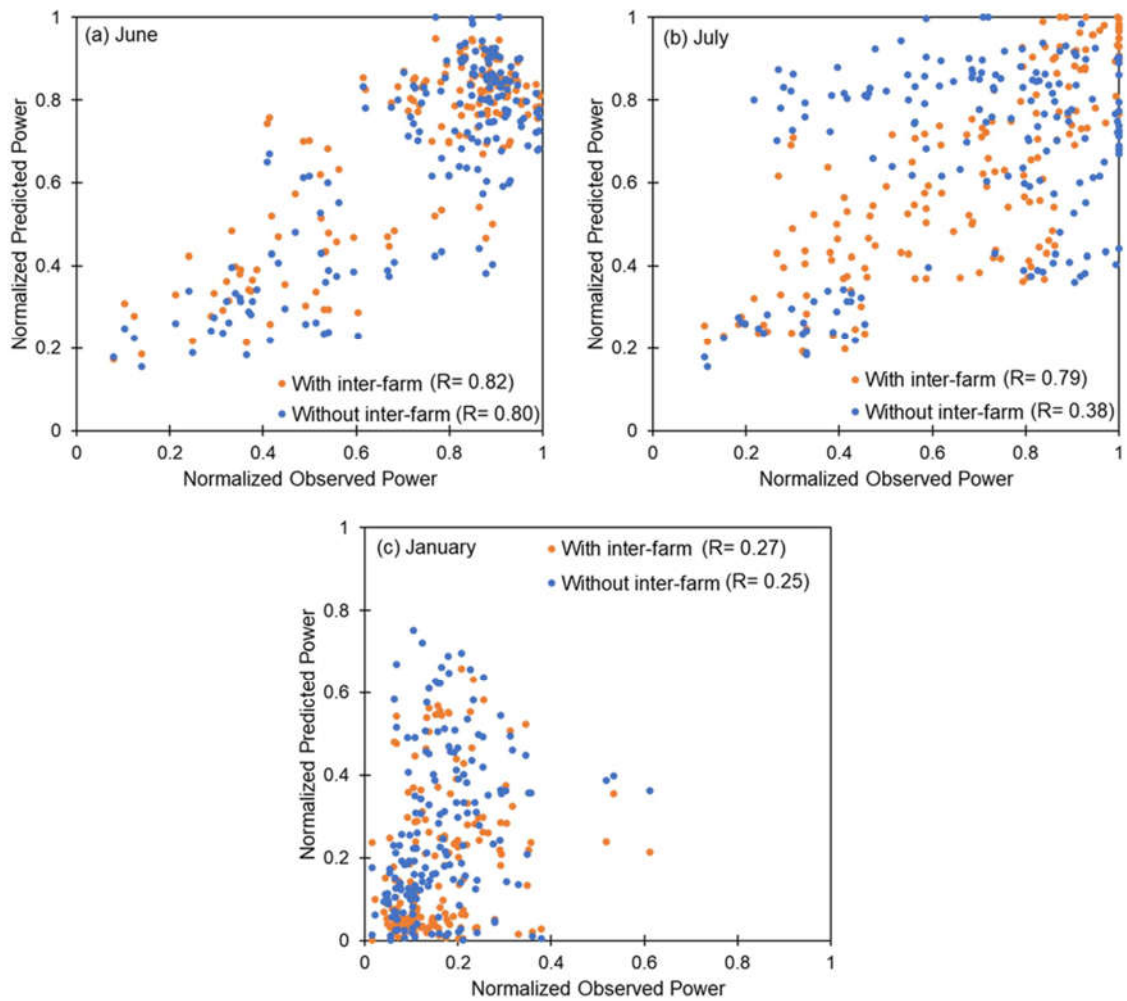


Figure 5.12 Comparison of predicted and observed total power generation of FFCEL for the months of (a) June, (b) July, and (c) January

Summary

MAE is reduced by 7.7 % in June at wind speed. A 14 % error reduction was observed in MAE in January. The WRF excellently estimated the wind directions. In June, a mean error of 13 % in NMAE is observed in all turbines in Case 1 and 11% was observed in Case 2. The forecasting skill of the WRF model was also assessed by another factor i.e. Pearson Correlation Factor. The WRF has a correlation of 0.82 in June and 0.27 in January.

Chapter 6

Conclusions

6.1 Conclusions

The discrepancies in the power prediction are observed due to inherent uncertainties in the WRF mesoscale model. Like other NWP models, the WRF only estimates the atmospheric interaction with the topography of the area by simplifying the physical process [1]. Error in the prediction also comes from the inadequacies of physical parametrization which leads to inability NWP models to successfully solve the sub-grid-level issues and also the skill of interpolation is affected. Not selecting the right initial and boundary conditions for the model also lead to the error in the forecast in NWP models. Error in wind speed is tripled, while power prediction in NWP, because of the cubic relation of wind speed and power. Therefore, high skill is required for wind energy forecasting [2].

1. A unique study of wind speed and power forecasting was done for the commercial-scale wind farm in the Province of Sindh, Pakistan. The test case wind farm is under the influence of inter-farm wake and extreme seasonal variation
2. In the span of simulations, the WRF overestimated the wind speeds when the mean wind speeds were high (summer), while underestimated the wind speed when the mean wind speeds were low(winter)
3. In the span of simulations, the WRF overestimated the wind speeds in the summer seasons, when the mean wind speeds were high. MBE was negative in summer, as the WRF underestimated the inter-farm wake mixing in the downstream wind. The WRF underestimated the wind speed in the winter season
4. The WRF was used with the Wind Farm Parametrization scheme to estimates the far inter-farm wakes while predicting wind resources. The simulation is run for two seasons i.e. summer and winter

5. The WRF, underestimated the inter-farm wakes in summer, while it overestimated the wakes in winter
6. Although the wind farm is located in complex terrain, the WRF estimated the inter-farm wakes with great accuracy
7. The WRF estimated the inter-farm wake effect in the forecasting with great accuracy. Although wind farms located in complex terrain, it is a major challenge to accurately simulate the complex atmospheric circulation.
8. The MAE in wind speed for the summer is improved up to 7.7%, while in the winter, a maximum of 14 % reduction in MAE was observed.
9. Wind direction for both the seasons was predicted by the WRF with great skill. In summer, a mean difference of only 33°. while in winter, the WRF predicted mean wind direction of 105°, while the mean observed value was 80°
10. The mean NMAE of power in each turbine was improved while considering interfarm wakes. In summer, 15 % improvement was observed in mean value, while in winter, mean value improvement of 26 % was observed.

6.2 Future Research Work

This study opens the gate for abundant research in the future. Some of the suggestions are

- a) Coupling CFD with the mesoscale models can be used for wind resource prediction, for accurate estimation of intra-farm wakes
- b) A hybrid model, coupling statistical model with the NWP model can be used to decrease the computational load on computers
- c) Wind farm optimization study can be carried out, with the wind farm parameterization scheme used to calculate far wakes
- d) The WRF can be used for the wind resource forecasting for the wind farm in urban areas
- e) The WRF can be used to validate wake models by comparing LES with the wake model in the WRF and empirical model

Reference

- [1] D. Carvalho, A. Rocha, C. S. Santos, and R. Pereira, “Wind resource modelling in complex terrain using different mesoscale-microscale coupling techniques,” *Appl. Energy*, vol. 108, pp. 493–504, 2013.
- [2] F. Cassola and M. Burlando, “Wind speed and wind energy forecast through Kalman filtering of Numerical Weather Prediction model output,” *Appl. Energy*, vol. 99, pp. 154–166, 2012.

Chapter 7

Research exchange Work

7.1 Lidar Lab in ASU

I spent one semester in the Lidar Lab of Dr. Ronald Calhoun at Arizona State University at Tempe Campus. There I studied the working and applications terrestrial and airborne Lidar in the field of forestry, resource assessment, aviation, and unmanned vehicles. I have done the semester-long project entitled “Design and fabrication of an ultra-sonic anemometer”, using the Arduino and cheap ultrasonic sensors. I designed the schematic diagram of the project in EAGLE CAD. After I designed, I fabricated with the available resources is shown Fig 7.1(a) to make a finished product. Then I tested the fabricate anemometer Fig 7.1 (b) in the wind tunnel to validate the theoretical results.

7.1.1 Ultra-Sonic Anemometer

An Ultra-Sonic Anemometer is a device which is used to detect and measure the speed of wind and its direction with greater accuracy than a mechanical anemometer. A mechanical anemometer uses abrasion or physical touch of wind on its cup shaped body, that decreases its precision and accuracy. But the ultra-sonic anemometer uses sound waves for wind speed measurements. A lidar works similar to the Ultra-Sonic anemometer, there are some differences such as Lidar uses light waves, and obviously it does not require any medium to pass, higher clock speed to respond, but the ultra-sonic anemometer uses lower speed clock.

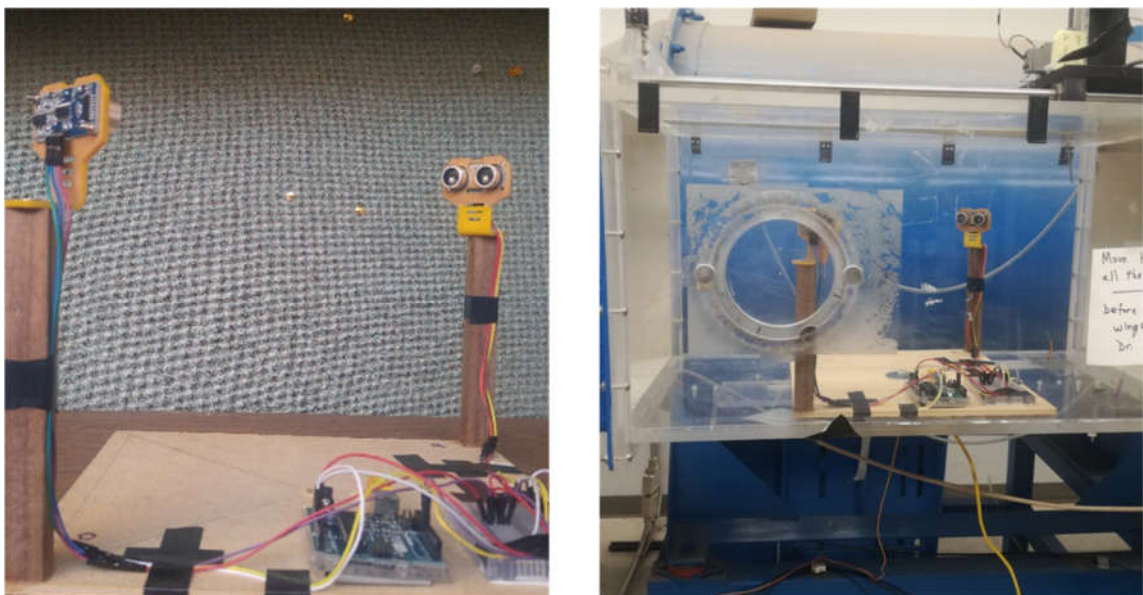


Figure 7.1(a) Fabricated ultrasonic anemometer (b) Testing in the wind tunnel

The validation results are shown in Fig 7.2.

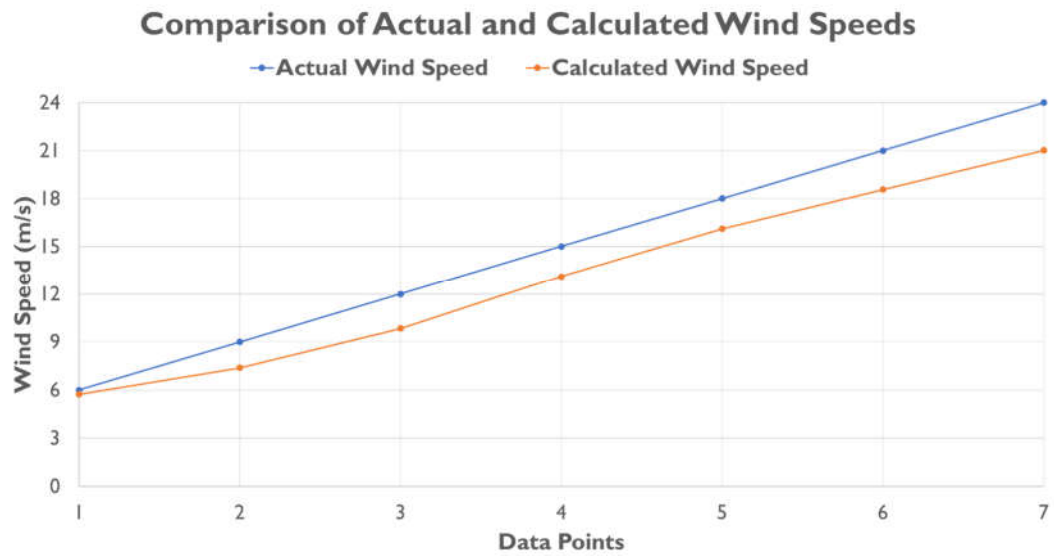
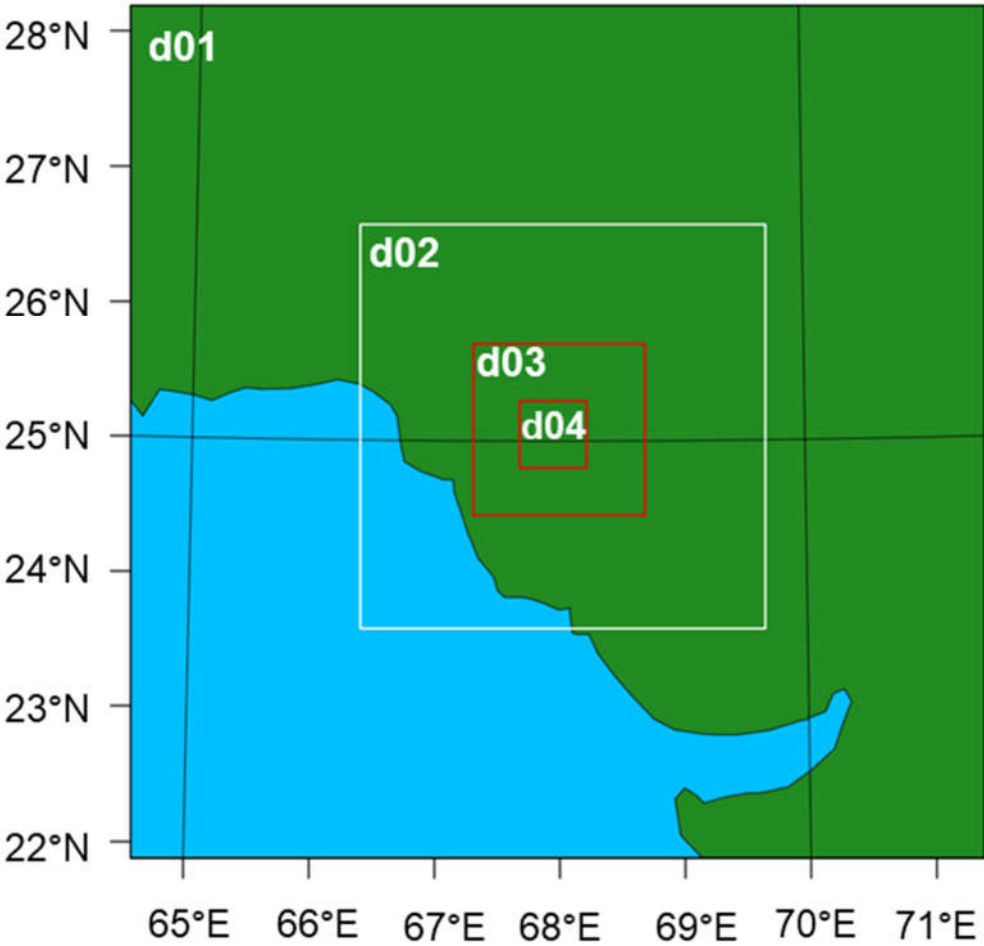


Figure 7.2 Speed variation ultrasonic anemometer with actual data

Chapter 8

Appendices

Appendix A: WRF Preprocessing System Domains



Wind Speed and Power Forecasting of a Utility-Scale Wind Farm with Inter-Farm Wake Interference and Seasonal Variation

Raja M. Asim Feroz, Adeel Javed ¹, Abdul Haseeb Syed, Syed Ali Abbas Kazmi

U.S.-Pakistan Centre for Advanced Studies in Energy, National University of Sciences and Technology, H-12 Islamabad, Pakistan

Abstract

Forecasting skills for a wind farm would significantly degrade if the complex wake effects of the upstream wind farms are excluded, especially when they are spatially close to each other. In this study, the Weather Research and Forecasting (WRF) model has been used to predict wind speed and power for a wind farm in Pakistan in the presence of wake interference from neighboring wind farms for two different seasons. Forecasting is done for two different cases i.e. without and with inter-farm wake effects, and different statistical error parameters were evaluated based on the real observations. A significant reduction in errors was observed in the latter case. For instance, the mean absolute errors in wind speed prediction were reduced by 7.7% and 14% in June (summer) and January (winter) respectively, by the inclusion of inter-farm wake effects. Similarly, an improved forecast of power output was obtained by incorporating the interaction of upstream wind farms i.e. a reduction of 15% and 26% in the normalized mean absolute error in power output values was observed for June and January, respectively. However, the prediction accuracy of power output substantially deteriorated in the winter season.

Keywords: wind farm; energy forecasting; wake interference; seasonal variation; mesoscale simulation

1 Introduction

There has been a remarkable growth in renewable energy generation over the past few years due to lower costs, government incentives, economic growth, and environmental concerns emerging from the utilization of traditional fossil fuels. An increase in wind turbine capacity factors and lower production costs over the last two decades have made wind energy an effective source of renewable energy. Global wind-generation installed capacity has increased from 7.5 GW in 1997 to 564 GW in 2018 with electricity generated

¹ Corresponding author, Email: adeeljaved@uspcase.nust.edu.pk

by wind energy resources accounted for 16% of the electricity generated by total renewable sources in 2016 [1]. Unlike traditional resources, the wind has unique characteristics as it varies substantially in the spatial domain along with temporal, diurnal, and seasonal variations. Therefore, wind energy production rate fluctuates more strongly than traditional fossil fuel sources of energy and other renewable sources. Intermittency of wind poses a huge risk for energy planning of electrical grids i.e. baseload management, managing demand and supply gap, and maintenance issues of wind farms, which can lead to a great economic loss if not anticipated. To make wind energy a reliable source for power generation, a dependable forecast is imperative. To forecast wind speed at different time horizons is a main concern for the wind energy planners. The benefits of wind power forecasting lie in the reduction of imbalance charges and penalties, grid maintenance issues, efficient project management planning, operational issues, and advance energy trading in the market.

The current techniques for wind speed and power forecasting mainly include statistical and physical methods. Statistical methods are utilized for very short-term predictions. These models are supposed to alter the model parameters based on the difference between predicted and past values, as these models are auto recursive [2]. An immense range of time series models has been proposed for statistical wind speed on various averaging intervals. Such models include forecasting time series using Kalman filters [3], ARMA (Autoregression moving average) functions [4], functions built using artificial neural networks [5]-[6], the fuzzy logic method [7], and Box-Jenkins models [8]. The forecasting skills of these models depend on the reliability [9] of the past data sets and the number of observed points (resolution) in those data sets. [10] demonstrated that there are many difficulties in the forecasting of energy demands using historical data points. As the lead time of wind-speed forecasting increases, the precision of statistical models degrades immensely.

For the wind speed forecasting of more than 6 hrs time horizon, physical models give an excellent estimation of wind energy resources, for instance, NWP (Numerical Weather Prediction) models [11]-[12]. Physical models such as NWP use weather and meteorological data for wind speed prediction [13]. NWP models are very effective models, as these solve the numerical equations of conservation of mass, energy, and heat on the real-locations and geographical grids points in all three dimensions. These models include the effect of latitude, longitude, and elevation of certain locations, and several other factors such as roughness and effect of topography. NWP models have certain merits over statistical models: these can scale-down wind speed to the turbine-hub height, give high resolution in vertical and horizontal domains, and do not have missing data amount [14]-[15]. These models are also used to produce the wind farm layout, speed in the local area, and power curves of the wind turbine on the farm. NWP models use interpolation techniques to scale-down wind speed by also using the terrain account of the wind farm. Collecting information regarding the description of the terrain is one of the most difficulties in the implementation of physical models.

Various studies have been conducted on wind speed and power forecasting for sites and wind farms all over the globe. For instance, stochastic and hourly wind speed forecasts in Jamaica employed past data to produce real-time series which was validated with the observed data [8]. The physical method of forecasting was utilized to predict wind speeds for the turbines in the Pomeroy, Iowa wind farm, USA [16]. Coupling mesoscale models with microscale models such as Computational Fluid Dynamics (CFD) and WindSim were some methods applied for the wind prognostication in wind farms of Nygard, Norway [17], and Manisa, Turkey [18] respectively. Some studies involved models that are a combination of physical and statistical methods, also referred to as hybrid methods, to predict wind characteristics. For instance, [19] utilized the Kalman filter, and [20] employed a genetic algorithm to clean out the physical model output for wind farms in Awaji, Japan, and Satavento, Galicia, respectively. These studies include the forecasting time horizon ranging from 24 to 72 hours however did not consider the wake effects of wind turbines while forecasting wind characteristics.

The wind resource forecasting for a certain wind farm without the inclusion of intra-farm wakes (wakes produced from inside a wind farm) and inter-farm wakes (wakes produced by neighboring wind farms) would give overestimation in wind speed, which would ultimately produce large discrepancies in the power output because of the cubic relation between wind speed and power. Even a small forecast error in speed enhances error to three times in the wind power estimation [21]. Complex wakes to emerge from the vortex of wind turbines greatly reduce the wind resource for the downstream wind turbines and hence forecasting wind resources to encounter the characteristic intermittency should also cater to the holistic wake phenomenon to generate a reliable data. Wakes from commercial wind turbines can endure a minimum distance downstream of 8 to 10 times the turbine's rotor diameter [22]. Wakes have an adverse effect on wind power production which leads to an increase in the cost of electricity [23]. A study [24] analyzed the wind speed and power prediction under the influence of intra-farm wakes on a real onshore wind farm and found out a 0.5% loss in wind resource even 17 km downstream of a wind farm. Two different techniques were used for evaluating the wake effects of neighboring wind farms by Lundquist et al. [25] and nearly 5% loss of generation in a downstream wind farm was observed. Li et al. [26] examined the impact of wakes on wind power prediction using Jensen and Larsen wake models and concluded a power loss of 35% in the downstream wind turbines. Both intra- and inter-farm wake flows affect the wind characteristics experienced by different turbines in an onshore wind farm. In addition to wake flows, uncoordinated design and development can result in less than the nominal distance between wind farms thus large errors in power output prediction. Moreover, spatial and geographic parameters that influence the local atmospheric boundary layer must be considered while forecasting wind speeds in complex terrain.

Wind turbines wake estimation models range from analytical to numerical, and mesoscale to microscale models. All these methods have their own merits and also come with some restraints. Several past studies have evaluated the accuracy of wake prediction methods under different types of operating conditions. Some famous analytical models are assessed

and compared by [27], who recommended that Jensen, and Xie and Archer wake models to be best for overall accuracy. [28] concluded that the accuracy of analytical wake prediction methods depends upon the downstream distance from a wind turbine. Modified 2D Jensen-Gaussian model [a more realistic analytical model] capture the wake effects from a wind turbine more accurately [29]. Most of the analytical methods do not include the effects of complex terrain and also ignore the dependency of wake models with respect to time i.e. these models consider speed deficit produced from a wind turbine as solely a function of distance, which underestimates the wake losses [30]. Numerical models like Computational Fluid Dynamics (CFD) models are although more accurate but are not used for wake analysis of whole wind farms for their high computational expenses [31]-[32]. CFD models use Navier-Stokes equations to compute the velocity deficit behind wind turbines. High fidelity Large Eddy Simulations (LES) results have been best in accordance with the measured data as compared to previously mentioned methods [33]. LES models are best suited for the near wakes as these models resolve hub and tip vortices near wind turbine blades. But LES is not suitable for resolving the wake flows emerging from whole wind farms due to excessive computational power required.

Fitch et al. [34] developed a Wind Farm Parameterization (WFP) scheme that resolves wind turbine wakes at the mesoscale level. In this scheme, wind turbines act as a source of drag and turbulent kinetic energy to the oncoming wind. This leads to a loss in momentum and a wind speed deficit based on the wind turbine thrust and power curve data provided by the manufacturer. This WFP scheme is implemented in a NWP model: the Weather Research and Forecasting (WRF) model [35] which is a current state of the art modeling tool developed on the MM5 model. The WRF uses terrain information and the eulerian based specification for the particle flow coordinate model in wind speed forecasting. To enhance the interaction of the atmosphere with the terrain of the area, the WRF employs microphysics parametrization schemes, long and short-wave radiations, planetary boundary layer schemes, cumulus process, and surface processes. The model uses physical parametrization to resolve the complex processes to predict temperature, wind speed, water vapors over real three-dimensional domains [36]-[37]. [16], and [38] used the WRF model to evaluate wind speed on the turbine-hub height. The WRF model has the excellent capability to predict wind speed and can also predict wind direction over the complex terrain [39], [15], [40]. Like other NWP models, the WRF model can perform simulations with a resolution of fewer than a hundred meters. The WRF model integrated with the WFP scheme has the ability to account for the drag and turbulent mixing of the upwind wind farm and can evaluate the irregularities of those wakes without using excessive computational resources unlike LES [25].

In this study, the authors focus on a utility-scale wind farm located in a complex terrain that is under the influence of wakes emerging from neighboring, closely spaced, upstream wind farms. The test case wind farm also experiences extreme variations in the wind direction over different seasons. The wind speed and power of the said wind farm will be predicted using the WRF mesoscale model by including the intra- and inter-farm wake effects, and the effect of seasonal variation on the prediction accuracy will be evaluated.

The test case wind farm lies in the province of Sindh, Pakistan. The main objectives of this study are (a) short-term wind forecasting of the wind farm under the influence of inter-farm wakes, (b) evaluation of variation in wind speed forecast accuracy under seasonal changes, (c) total power prediction of the wind farm, and (d) error analysis in power prediction of individual turbines.

Section 2 of this paper details the technical specifications of wind farms under study, the methodology applied to obtain forecast data, the configuration of the WRF model, and information related to geographical domains and physics schemes. Error parameters used to check the validity of the forecasted wind speeds and power are also described in the same section. Section 3 discusses the forecast results obtained by the WRF model and their comparison with the observed data of met mast and wind turbines in the wind farm. This section also discusses the errors in the power prediction of individual wind turbines under two different seasons. Section 4 presents the summary and main conclusions that emerged from this research work.

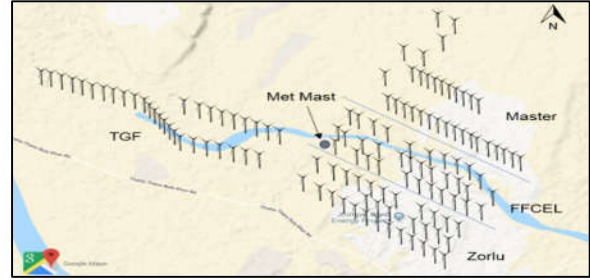
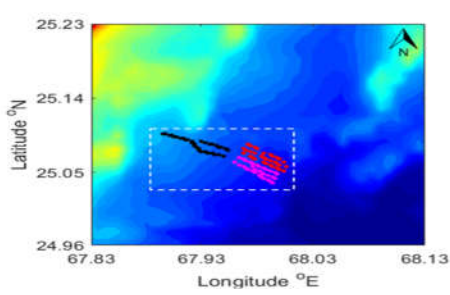


Figure 1. Terrain altitude of Jhimpir,

Figure 2. Wind farms layout in the

2 Methodology

2.1 The test case wind farm

The FFC Energy Limited (FFCEL) wind farm is located in the Jhimpir region of the southern province of Sindh, Pakistan. The FFCEL wind farm is under operation since 2013. It contains 33 x Nordex S77 wind turbines, with each turbine having 1500 kW of maximum rated power. The total wind power production capacity of the FFCEL wind farm is 49.5 MW. The hub height and rotor diameter of all the turbines are 80 m and 77m, respectively. Fig. 1 depicts the terrain in which wind farms and met mast lies in the Jhimpir area [41]. The test case wind farm lies on uneven terrain, with uncoordinated wind farms surrounding it and experiencing extreme seasonal variations, that make this wind farm a unique case to study. The FFCEL wind farm is surrounded by three neighboring wind farms operated by Zorlu in the South-West, Three Gorges First (TGF) wind farm in the North-West, and Master Wind Energy limited (MWEL) in the North-East side (Fig. 2). The technical details of the four wind farms are shown in Table 1. Fig. 3 [41] illustrates that the two most dominant wind directions in the Jhimpir region are South-west and North-East which occur in Summer and Winter, respectively. In the summer months, the main hindrances to the FFCEL wind farm for a cleaner wind resource are the Zorlu and

the TGF wind farms, while in the winter season, hindrance comes in the form of the Master wind farm. As the wind changes its direction in the two most dominant seasons of the year, these upstream wind farms are the source of wind turbines wakes to the test case wind farm FFCEL, that is why wind speed forecasting is done for two seasons in this study while catering to the wind direction and wake flows of the upstream wind farms.

Table 1. Wind farms’ technical specifications

| Wind Farm | FFCEL | Zorlu | | TGF | Master |
|-------------------------------------|-------------|-------------------|------------------|----------------------|-------------|
| Wind Turbine Model | Nordex S77 | Vestas V90 1.8 MW | VensysV62 1.2 MW | Goldwind GW77 1.5 MW | GE 1.6 XLE |
| No. of Wind Turbines | 33 x 1.5 MW | 28 x 1.8 MW | 5 x 1.2 MW | 33 x 1.5 MW | 33 x 1.6 MW |
| Rotor diameter (m) | 77 | 90 | 62 | 77 | 82.5 |
| Hub Height (m) | 80 | 80 | 69 | 85 | 80 |
| Power Density (m ² / kW) | 3.11 | 3.5 | 2.5 | 3.1 | 3.6 |
| Distance from the FFCEL (---) | - | ~790 | | ~1390 | ~800 |

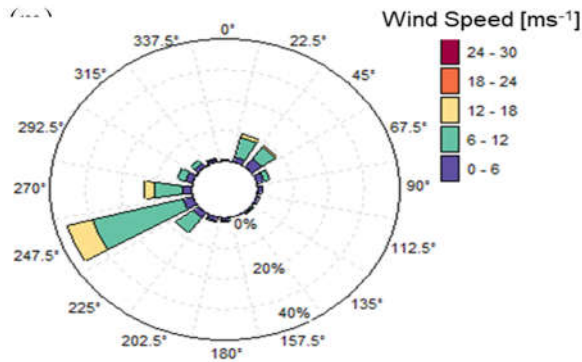


Figure 3. Observed wind speeds and directions for the year 2018 in the Ihimpir

2.2 WRF model configuration

The WRF model version 4.1 is used for this study, which is the latest version and is commonly used for the operation of weather forecasting and atmospheric research [35]. The methodology applied to obtain the wind speed and power forecast for the FFCEL wind farm using the WRF model is presented in Fig. 4. The Moderate Resolution Imaging Spectroradiometer (MODIS) geographical data with a high resolution of 30 arc seconds is used as a boundary condition in the forecasting model. The Global Forecasting System (GFS) [42] data of grid/scale 004 (0.5°) is used as an initial condition. This data was obtained from the National Centers for Environmental Prediction (NCEP) which updates

it after 6 hrs interval. The GFS data from the previous day run is used as the forecasting tool for future prediction. Both data sets are freely available for research purposes. The WRF model employs Arakawa C-grid staggering with a mass-based terrain-following vertical coordinate to solve for different atmospheric parameters using Elurian based conservation equations of mass, momentum, and energy. Wind turbine parameters are also fed into the model that include geographical coordinates of wind turbines, power curve, and thrust curve data. The model forecasts different atmospheric parameters by interpolating the gridded initial data on the domains' grid cells at each time interval. Parameters like wind speed at the hub height can be extracted in the post-processing phase using data interpolation in the grid cells where wind turbines are located. The forecasted wind speed data is then compared with the data observed from the nacelle mounted anemometer at each wind turbine.

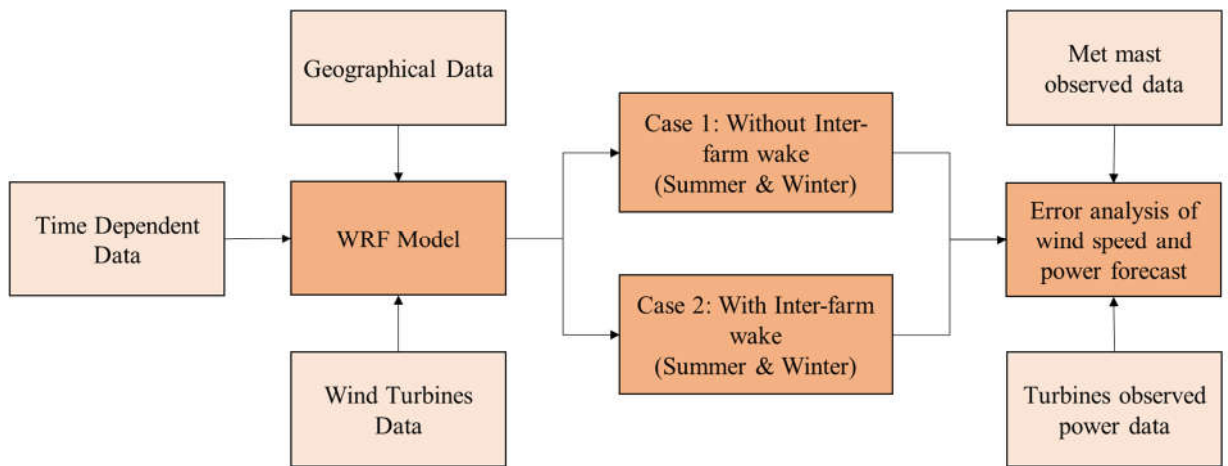


Figure 4. Methodology applied for the current

The resolution of spatial grids can be increased up to a few hundred meters in the WRF model. The model is set with four two-way nested domains with an advanced horizontal resolution of 9000, 3000, 1000, and 333 m. While setting the domains, requirements for the configurations of the domains were met, as proposed by Warner [43], including the parent (d01) and three nested grids (d02, d03, d04). Domains resolution, grid points, and vertical levels are listed in Table 2. The innermost domain d04 is centered at 25.075 ° N and 67.972 ° E (Fig. 5). The highest resolution domain covers an approximate area of 55 km x 55 km, which gives suitable information about the meteorological effects which are occurring locally near the wind farm. The 333 m inner-most domain's resolution gives more than adequate information about the wind farm and topographical characteristics of the terrain [24], [39].

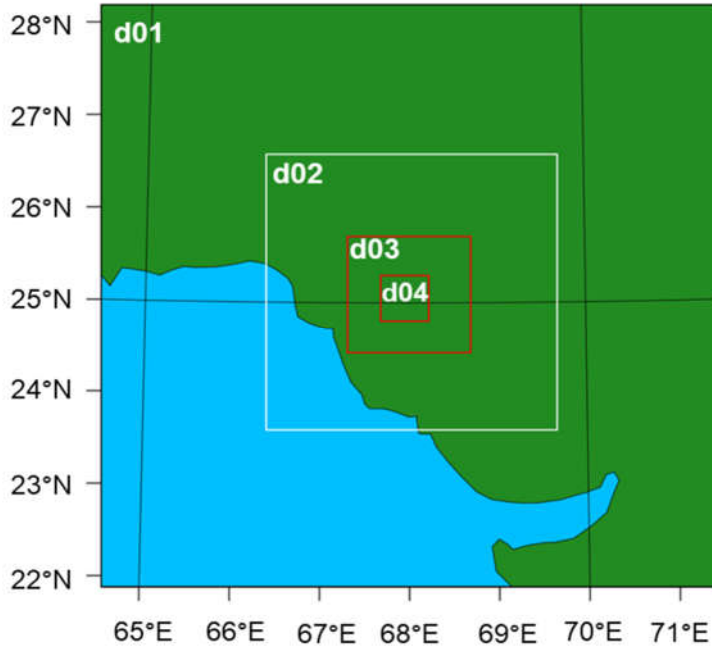


Figure 5. WRF model nested domains. D04 represents the area of interest and has the highest

Physics schemes options include a newer version of rapid radiative transfer model longwave [44] and rapid radioactive transfer model shortwave was used. New Thompson et al. [45] was used to resolve the microphysical processes, the unified Noah model [46] resolved the land surface fluxes. Turbulent phenomena occurring near the boundary layer were resolved by the Mellor-Yamada (MYNN) [47] as the planetary boundary layer(PBL) scheme. Convection which is occurring during the interaction of the atmosphere is characterized by the Tiedtke scheme [48]. The WFP scheme developed by Fitch et al. [34] is used to evaluate the wind turbines’ wake and the effect of those wakes on the wind farm’s power production. This scheme represents a wind turbine as a source of turbulence that converts kinetic energy from the wind into useful energy (extracted by the turbine) and turbulent kinetic energy that produces downstream turbulence. The vertical shear produce near the boundary layer of the surface by the momentum sink is accounted for by the MYNN. The effects of buoyancy and stability after the momentum sink and turbulent mixing is also characterized by the planetary boundary layer scheme MYNN.

Table 2. WRF model domains’

| Domains | 1 | 2 | 3 | 4 |
|-----------------|----------|-----------|-----------|-----------|
| Grid Points | 79 x 79 | 112 x 112 | 142 x 142 | 166 x 166 |
| dx=dy (km) | 9 | 3 | 1 | 0.33 |
| Vertical Levels | 40 | 40 | 40 | 40 |

2.3 Simulations setup

To evaluate the influence of wind farms' wake effects on the accuracy of wind speed forecasting, two different sets of simulations were designed. One set included the inter-farm wake effects emerging from the three neighboring wind farms, while the other set catered only the intra-farm wake effects of FFCEL and ignored the inter-farm wakes. Both sets were simulated for 7 days period in two summer months of June and July and a winter month of January. The wind characteristics remarkably alter between the two seasons so the effect of seasonal variation on forecasting accuracy was essential to study. The wind speed and power results obtained from this study were also compared with the observed data obtained from the FFCEL wind farm. The forecasted wind speed at the turbine hub height is then used for power calculation using the power curve provided by the wind turbine manufacturer.

Table 3. Simulations setup

| Season | Case 1: Without considering inter-farm wakes | | Case 2: With considering inter-farm wakes | |
|--------|--|----------------------------------|---|----------------------------------|
| | Beginning Date | End Date | Beginning Date | End Date |
| Summer | 1 Jun 2018, 0000 hrs. UTC | 8 June 2018, 0000 hrs. UTC | 1 June 2018, 0000 hrs. UTC | 8 June 2018, 0000 hrs. UTC |
| | 1 Jul 2018, 0000 hrs. UTC | 8 July 2018, 0000 hrs. UTC | 1 July 2018, 0000 hrs. UTC | 8 July 2018, 0000 hrs. UTC |
| Winter | 1 Jan 2019, 0000 hrs. UTC | 8 Jan 2019, 0000 hrs. UTC | 1 Jan 2019, 0000 hrs. UTC | 8 Jan 2019, 0000 hrs. UTC |

The real-time observed data recorded by the met mast, and the wind speed and power data obtained from the turbines are utilized to assess the accuracy of the forecasting model. Wind speed at each turbine is collected by the anemometers located on top of the nacelle. This data was available at a frequency of 10 minutes intervals where each value represented an average data of 10 mins. Nacelle wind observations give a more real scenario at the turbine hub height [19].

Different statistical parameters are computed from the output data of simulations to analyze the accuracy of forecasting ability. Mean absolute error (MAE) represented in Equation 1, is the most important parameter used to check the precision of the prediction skill of the model. It represents the absolute average error between observed and forecasted values. To check whether the model is under or overestimating the forecasted data from observed value, there is another parameter mean bias error (MBE) represented in Equation 2, which gives adequate information about the sensitivity of the model. Equation 3 represents the root mean square error (RMSE), it is the measure of the absolute deviation of the predicted values from the observed values. For wind power production, the normalized mean absolute error (NMAE) (Equation 3) is used which represents the percentage of error in the power production of each wind turbine. In Equations 1-4 [24], i represent the observation in time, n is the total number of observations, f and Obs are

predicted and observed values, respectively. For MAE, MBE, and RMSE f and Obs are wind speeds, while for NMAE these variables represent power output values.

$$MAE = \frac{1}{n} \sum_{i=1}^n |Obs_i - f_i| \quad (1)$$

$$MBE = \frac{1}{n} \sum_{i=1}^n (Obs_i - f_i) \quad (2)$$

$$RMSE = \sum_{i=1}^n \sqrt{\frac{(Obs_i - f_i)^2}{n}} \quad (3)$$

$$NMAE = \frac{\frac{1}{n} \sum_{i=1}^n |Obs_i - f_i|}{NP} \quad (4)$$

3 Results and Discussion

3.1 Wind speed and direction forecast analysis

Wind speeds from both cases i.e. Case 1: without inter-farm wakes and Case 2: with inter-farm wakes were compared with the met mast data which is situated adjacent to the FFCEL wind farm. Wind speed variation for the first seven days in June 2018, July 2018, and January 2019 is presented in Fig. 6, where the trends for both Case 1 and Case 2 follow the observed values.

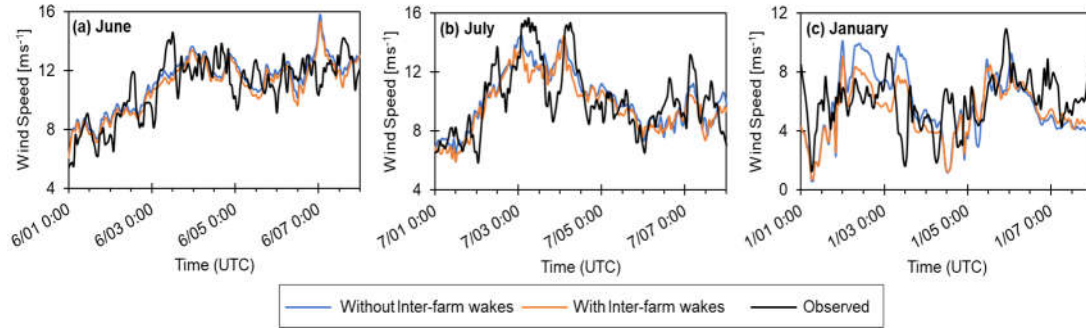


Figure 6. Temporal variation between forecasted (without and with inter-farm wake effects) and observed wind speed for the first week in months of (a) June,

The error analysis for wind speed forecasting in the region is presented in Table 4. A notable decrease in all the error parameters has been observed for Case 2 due to the inclusion of inter-farm wake effects. MAE for June was reduced by about 7.7% for Case 2. A significant improvement of 40% in the bias error (MBE) was recorded which is -0.85 ms^{-1} for Case 1 and it has decreased to -0.51 ms^{-1} for Case 2. RMSE values showed a little variation for the two cases and are reduced from 1.63 ms^{-1} in Case 1 to 1.52 ms^{-1} in Case 2. In July, the results of both cases show mixed results with minor differences. Insignificant improvement was noted for MAE and RMSE values which represent the deviation from the observed values. But a considerable decrease in MBE is found with an improvement of about 68%. Overall, the WRF model follows the observed trend with great accuracy. During January, the mean value of wind speeds is on the lower side than

in the summer months. WRF underestimated the wind speed, except for days 2 and 3 as represented in Fig 6(c). The MAE and RMSE values are higher as compared to the summer season but a reduction in errors is noted for Case 2 that includes wake effects emerging from neighboring wind farms. MBE gets increased and a positive deviation is observed in the forecasted values for Case 2. A considerable amount of 14% improvement was observed in MAE for Case 2 relative to Case 1, while MBE increases for Case 2 as the WRF overestimates the wake mixing. Even though prediction skills degrade with the increase in the lead time of the forecast, on the second day there are not many errors as compared to day one results for the summer season, and in both cases, discrepancies are very small. For the winter season, as the lead time increases, forecasting skill degrades significantly. Negative MBE for almost all turbines shows that underestimation of wakes by the WRF and overestimation of speed in the summer season and vice versa in the winter season.

Table 4. Statistical analysis of forecasted

| | | Case 1: Without considering inter-farm wake | | | Case 2: With considering inter-farm wake | | |
|--------|--------|--|-------------------------|--------------------------|---|-------------------------|--------------------------|
| | | MAE (ms ⁻¹) | MBE (ms ⁻¹) | RMSE (ms ⁻¹) | MAE (ms ⁻¹) | MBE (ms ⁻¹) | RMSE (ms ⁻¹) |
| Summer | June | 1.30 | -0.85 | 1.63 | 1.20 | -0.51 | 1.52 |
| | July | 1.34 | -0.57 | 1.66 | 1.32 | -0.18 | 1.64 |
| Winter | Januar | 1.87 | -0.15 | 2.42 | 1.59 | 0.25 | 2.02 |

Another crucial parameter to assess the forecasting model is the estimation of wind direction. The WRF predicted the wind direction for both cases with excellent similitude with the observed values of wind direction. Fig. 7 illustrates the prediction of wind direction using wind rose chart for Case 2 and those were then validated by the direction observed by the met mast located adjacent to the FFCEL. In June, the mean wind direction predicted by the WRF model is 222° while the mean observed direction is 247°. A mean error of 33° is observed for the whole week of June. 66% of the sample in the WRF data lies in the speed range of 10-13 ms⁻¹, while approx. 58% of the observed sample lies in the identical speed range. In July, the mean wind direction predicted by the WRF was 224° degrees and the observed wind direction was 241°, the mean error of 18° degrees was observed. Forecasting skill for wind direction of the WRF model enhanced in July. Approximately 67% of the WRF samples lied in the speed range of 10-13 ms⁻¹, while more than more 70% of observed samples lied in the same wind speed range. In January, similar to wind speeds, the errors in the wind directions were high. The mean predicted wind direction of the WRF and observed was 105° and 80°, respectively. The mean error in wind direction in the winter month came out to be 50°. More than 57% of predicted data by WRF lied in the wind speed of 7-10 ms⁻¹ while approximately 47% of observed samples lied in the exact wind speeds range.

3.2 Wakes Analysis of the wind farm

It can be inferred from Fig. 7 that in the Summer months of June and July, Zorlu and TGF wind farms act as upstream wind farms and a wind resource deficit for the FFCEL wind farm. Similarly, in the winter month of January, the Master wind farm acts as an upstream, wake producing wind farm for the FFCEL wind farm. Fig. 8 illustrates the wind speed contours in July when the wind approaches the Jhimpir region from the South-West direction. A significant decrease in wind resource available for the FFCEL can be observed for Case 2. Fig. 9 [41] further quantifies these wake losses in terms of percentage speed deficit contours, and speed deficit experienced by individual turbines in the presence of upstream wind farms. A speed loss of more than 12% was observed for the wind turbines located in the South-East region.

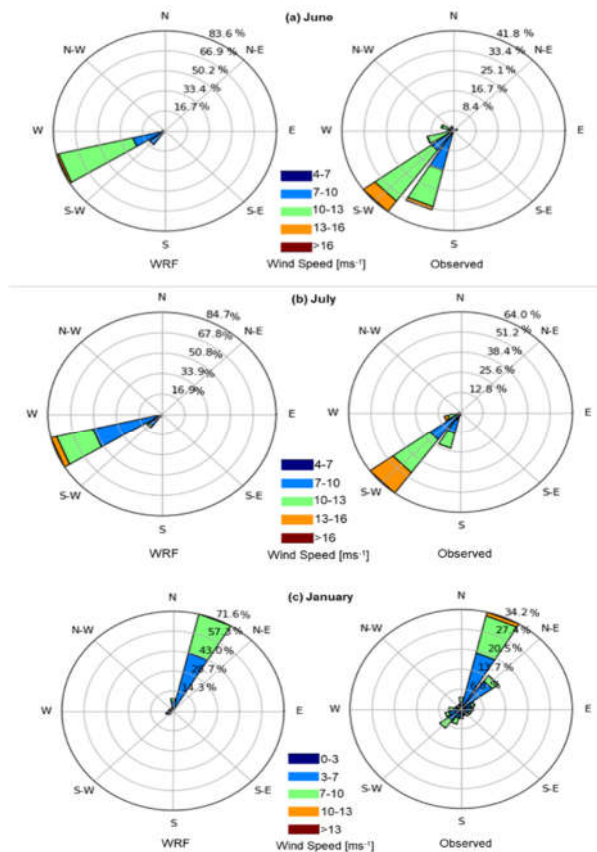


Figure 7. Comparison of predicted

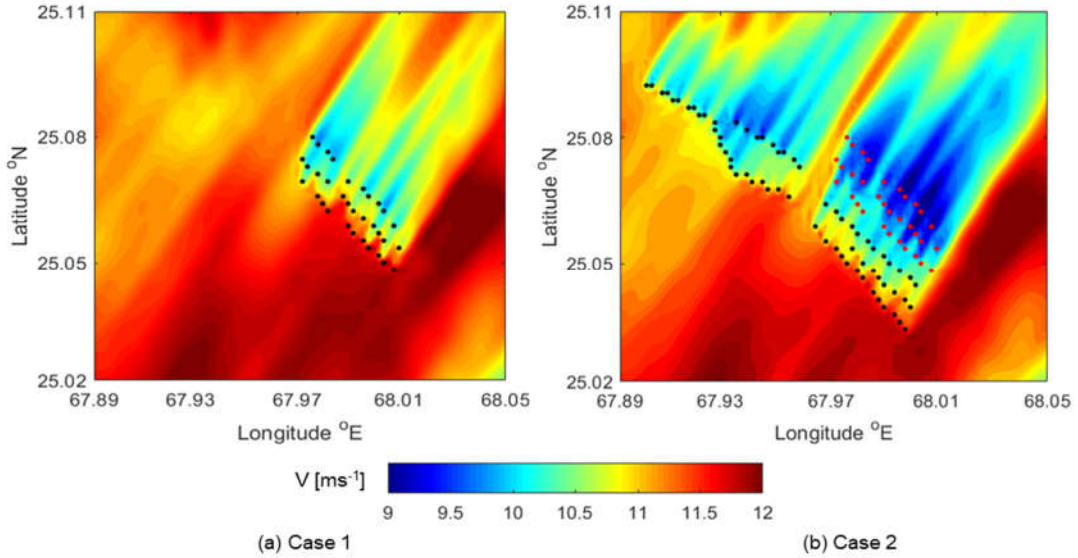


Figure 8. Wind speed contours during the Summer month of July when wind approaches the Jhimpir region from the South-West direction. Shown for (a) Without inter-farm wakes (Case 1) and (b) With inter-farm wakes (Case 2)

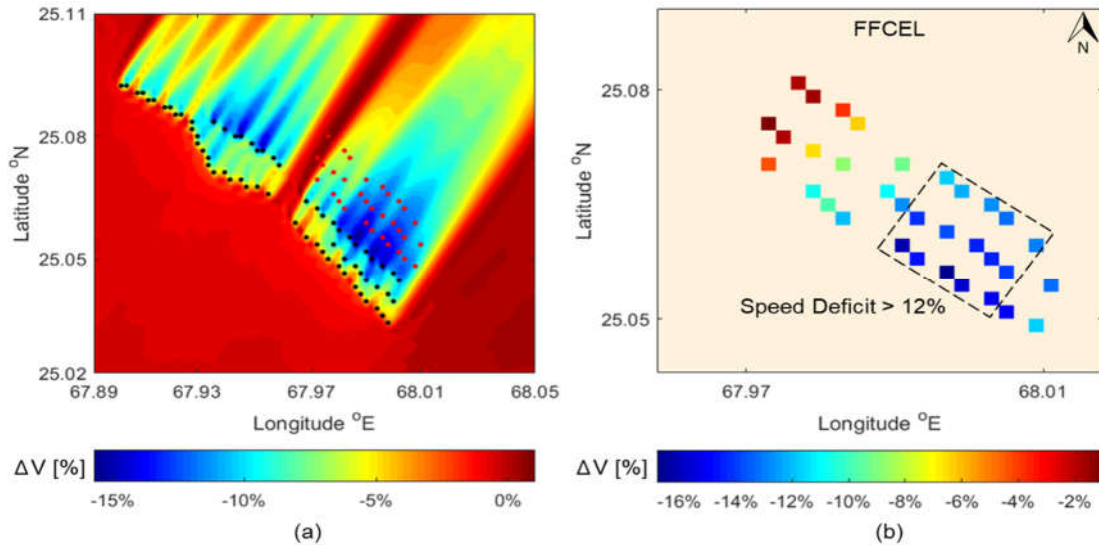


Figure 9. Speed deficit due to upstream wind farms on the FFCEL (a) Speed deficit contours (b) Speed deficit experienced by individual wind turbines

Using the data shown in Fig. 8 and Fig. 9, the wind turbines in FFCEL can be divided into two sets as shown in Fig. 10. Set A (turbines no. 1-12, 14-15, 33) of wind turbines is less influenced by the upstream wind farms wakes than the Set B (turbines no. 13, 16-32). Three wind turbines from each row in both sets were selected to analyze the wind speed and power variation experienced over seven days in June and January. Turbines number 1, 3, and 11 are present in 1st, 2nd and 3rd row, respectively in set A, while turbines number 22, 16, and 31 are from set B, and are present in 1st, 2nd and 3rd row respectively.

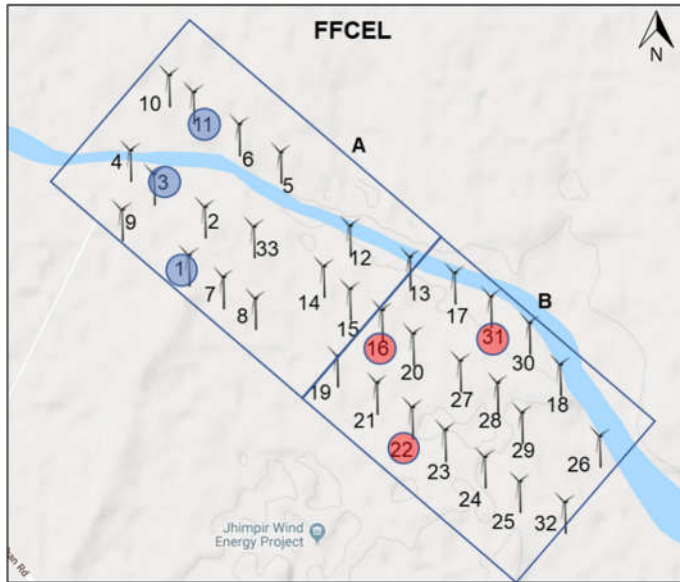


Figure 10. Wind farm layout, categorizing wind turbines in two sets i.e. A: under less influence of inter-farm wakes, B: under more influence of inter-farm wakes

Figure 11. represents the time-series graphs of wind speed prediction of the selected wind turbines for both Case 1 and Case 2, as well as the observed values for June. The symbol delta Δ in Fig. 11 and Fig. 12 represents the reduction in Mean Absolute Error (MAE) in ms^{-1} for Case 2 as compared to Case 1. The set A turbines 1, 3, and 11 show little improvement in the MAE, while the set B turbines 16, 22, and 31 show significant improvement in the MAE for Case 2. The forecasting accuracy is much improved in Case 2 for set B wind turbines because these turbines are under high influence of upstream wind farms' wakes and ignoring these wake flows can cause huge uncertainties. There is another parameter used to assess the prediction accuracy of a forecasting model known as the Pearson correlation coefficient (R). The WRF model showed a significant improvement in the correlation factor for Case 2 that includes the inter-farm wakes in wind speed forecasting. Wind speed prediction of the selected wind turbines for January (winter season) is demonstrated in Fig 12. Similar to the summer season, the improvement in the MAE for Set B wind turbines is higher. Master wind farm acts as the upstream wind farm as noticed from Fig 7. Although turbines in the set B are experiencing more inter-farm wakes, the prediction of wind speed using inter farm wake parametrization also significantly improves the forecasting skill of the WRF for the turbines in the set A. Although Δ in MAE for January shows improvement like the summer season, there is a slight change in R when wakes effects are included.

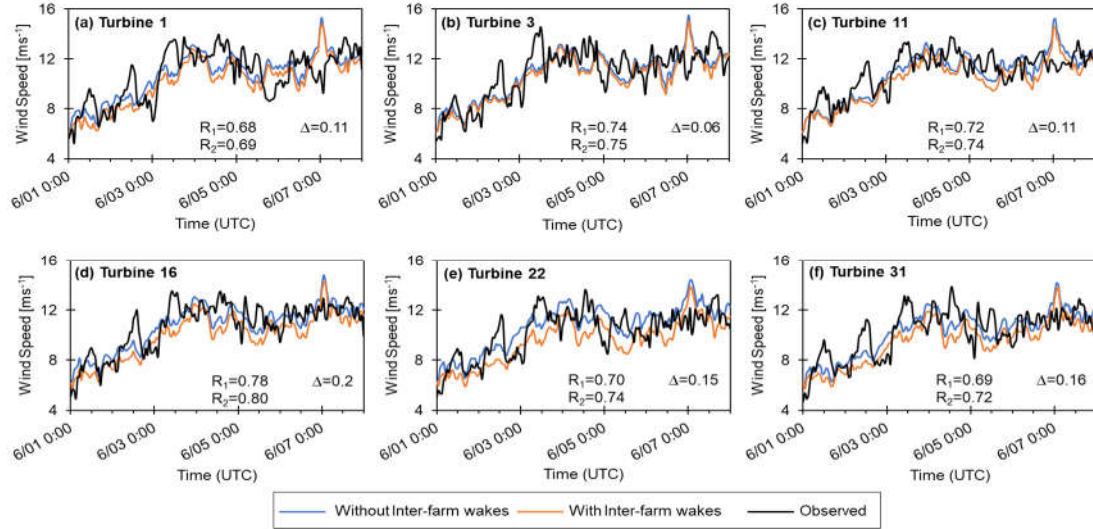


Figure 11. Wind speed forecasting analysis for the month of June. Set A turbines are presented in (a) Turbine 1, (b) Turbine 3, and (c) Turbine 11, whereas (d) Turbine 16, (e) Turbine 22, and (f) Turbine 31 present set B turbines. Δ represents the reduction in MAE

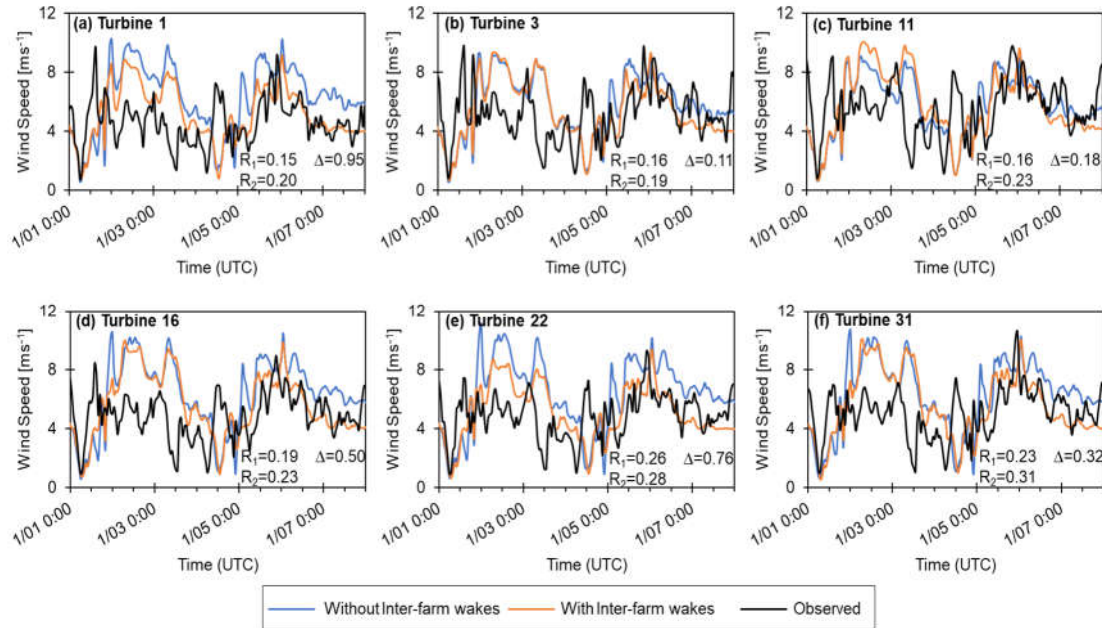


Figure 12. Wind speed forecasting analysis for the month of January. Set A turbines are presented in (a) Turbine 1, (b) Turbine 3, and (c) Turbine 11, whereas (d) Turbine 16, (e) Turbine 22, and (f) Turbine 31 present set B turbines. Δ represents the reduction in MAE in ms^{-1} for Case 2 as compared to Case 1. R_1 and R_2 represents the Pearson correlation for

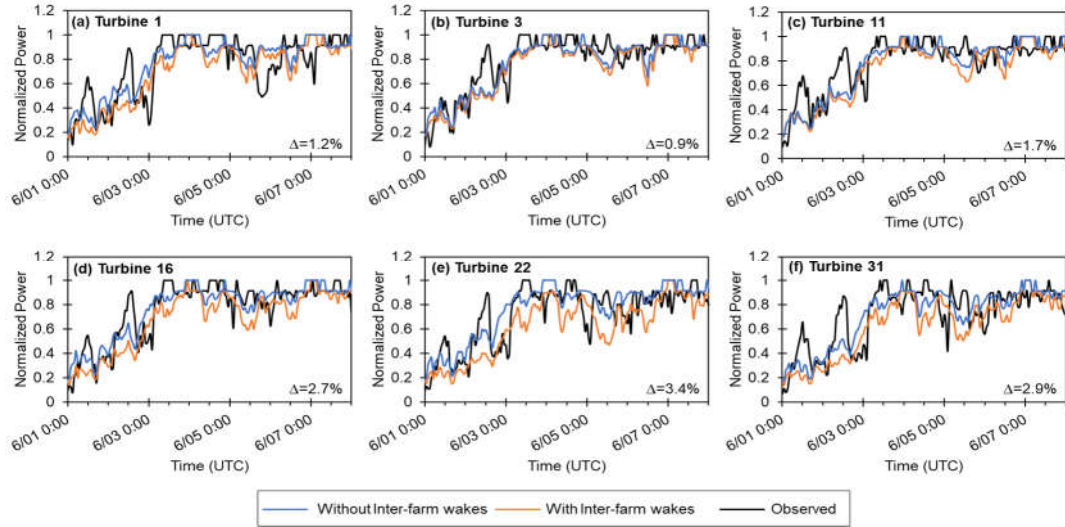


Figure 8-13. Wind power forecasting analysis for the month of June. Set A turbines are presented in (a) Turbine 1, (b) Turbine 3, and (c) Turbine 11, whereas (d) Turbine 16, (e) Turbine 22, and (f) Turbine 31 present set B turbines. Δ represents the %

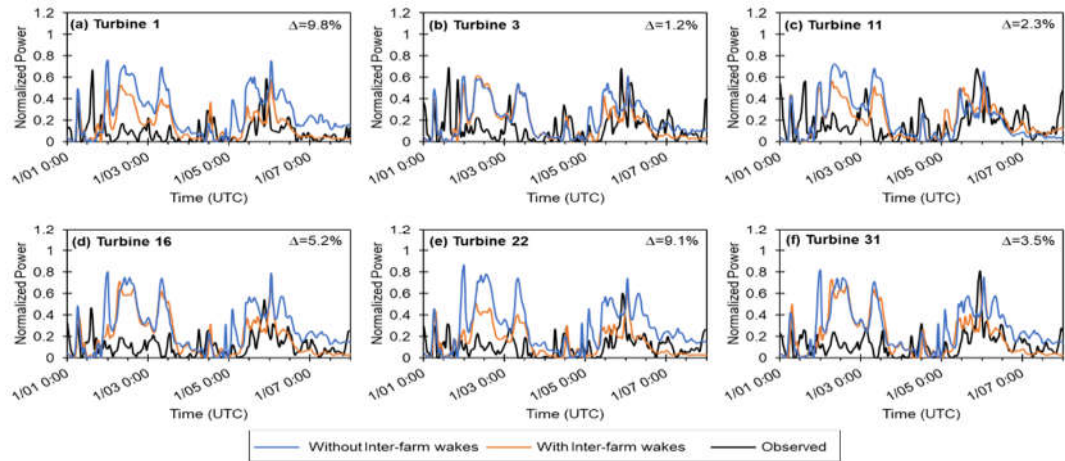


Figure 14. Wind power forecasting analysis for the month of January. Set A turbines are presented in (a) Turbine 1, (b) Turbine 3, and (c) Turbine 11, whereas (d) Turbine

The normalized wind power of the selected wind turbines from set A and set B predicted by the WRF relative to observed power for June is presented in Fig 13. The symbol delta Δ in Fig. 13 and Fig. 14 represents the percentage reduction in Normalized Mean Absolute Error (MAE) for Case 2 as compared to Case 1. Like speed, wind power forecast is significantly improved for set B turbines. It can also be seen in Fig 13, that even for the set A turbines, the power forecast is noticeably improved if wind speed forecasting is done using the WFP scheme. More than 2.7 % improvement of NMAE is observed for all the turbines in the set B when inter-farm wake effects are included in the forecast. Figure 14, presents the normalized power of the selected turbines in January. Although forecasted power data of all wind turbines experienced an improvement by the inclusion of inter-farm wake effects, it can be seen that the set B turbines have undergone more improvement

in forecasted power as compared to set A with an exception of turbine 1. More than 3.5 % improvement in forecasted power was observed in set B turbines using the inter farm wake parametrization.

3.3 Error Analysis of Individual Turbines

3.3.1 Mean Absolute Error

MAE in wind speed forecast of all 33 turbines in FFCEL wind farm is determined for both cases i.e. without and with inter-farm wake effects as shown in Fig. 15. MAE is relatively constant throughout the summer season, with a value of around 1.23 ms^{-1} for Case 1, and 1.09 ms^{-1} for Case 2. Among all the turbines for June, the maximum reduction of error occurs for the turbine 18 in Case 2 which is 30%. For July, the maximum reduction in error occurs for turbine 10 which is 39%. During the winter season, MAE for both the cases is higher as compared to the summer season, with an average value of 2.3 ms^{-1} for Case 1 and 1.8 ms^{-1} for Case 2. The maximum reduction in MAE occurs for turbine 19 in January in Fig 15 (c). Set B turbines (Fig. 10) showed a significant amount of MAE reduction for Case 2 in both summer and winter season. This indicates that these turbines are under high influence of inter-farm wake effects than Set A turbines, and ignoring the interference effects of neighboring wind farms can lead to substantial errors in wind speed forecasting.

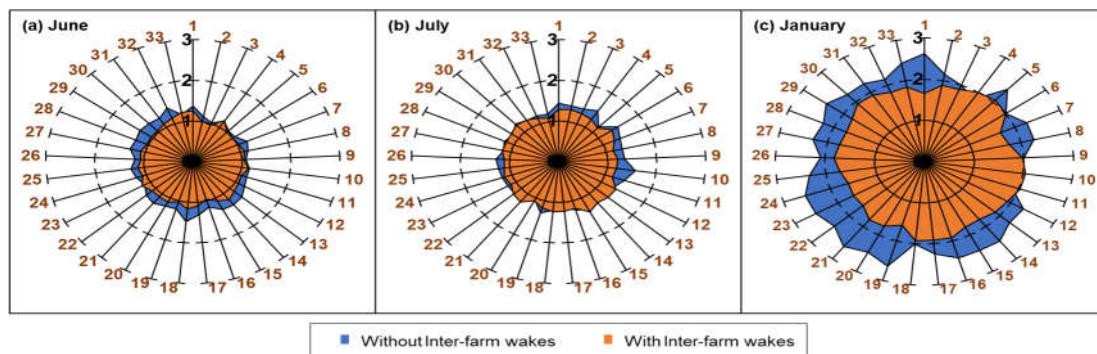


Figure 15. Comparison of mean absolute errors (MAE) of wind speed experienced by individual turbines for Case 1: Without inter-farm wake effects and Case 2: With inter-farm wake effects for (a) June, (b) July, and (c) January. Error values are higher in January as compared to the summer months.

3.3.2 RMSE

The mean value of RMSE (see Fig. 16) is 1.53 ms^{-1} for Case 1 and 1.36 ms^{-1} for Case 2 during June, and the maximum reduction in error of 20% is observed for the turbine 18. For July, the value of RMSE for Case 1 is 1.53 ms^{-1} and for Case 2 it is 1.36 ms^{-1} and the maximum reduction in error occurs for the turbine 10 which is 23%. Like MAE, RMSE for the winter season is on the higher side for both the cases, having average values of

about 2.7 ms^{-1} and 2.2 ms^{-1} for Case 1 and Case 2 respectively. During the winter month, the maximum reduction of 30% in RMSE is observed for turbine 19.

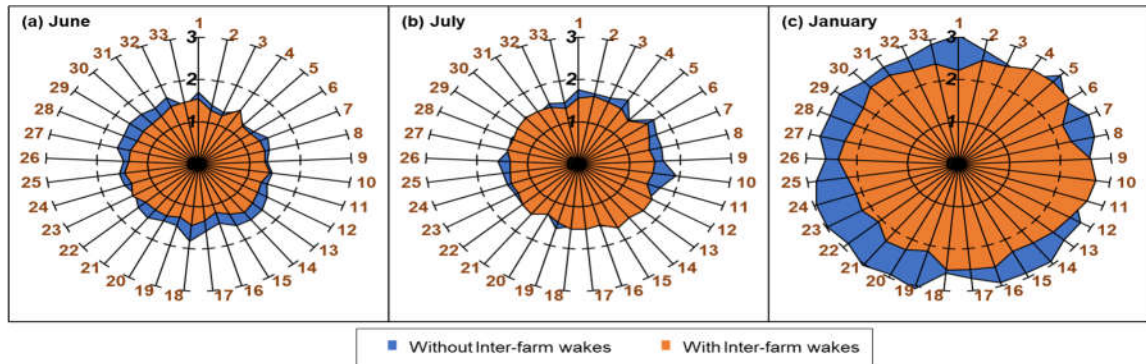


Figure 16. Comparison of root mean square error (RMSE) values of wind speed experienced by individual turbines for Case 1: Without inter-farm wake effects and Case 2: With inter-farm wake effects for (a) June, (b) July, and (c) January.

3.4 Power prediction analysis

The total power generation of the FFCEL wind farm is evaluated and compared with the observed power output of the wind farm. Fig. 17 illustrates the forecasted and observed power values for seven days in June 2018, July 2018, and January 2019. The WRF model underestimates the power prediction in June (Fig. 17(a)). During the first two days of the month, power prediction shows significant errors from observed values because wind speeds are also underestimated during the same period. In July, the WRF model predicted the power generation with high accuracy throughout the week except for the last two days when it underestimated the power prediction (Fig. 17(b)). In January (Fig. 17(c)), the WRF overestimated the power prediction of the wind farm most of the time and displayed a higher deviation from observed values than the summer months. Overall, a high correspondence between the power forecasted in Case 2 (with inter-farm wakes) and the observed power can be seen in all three months.

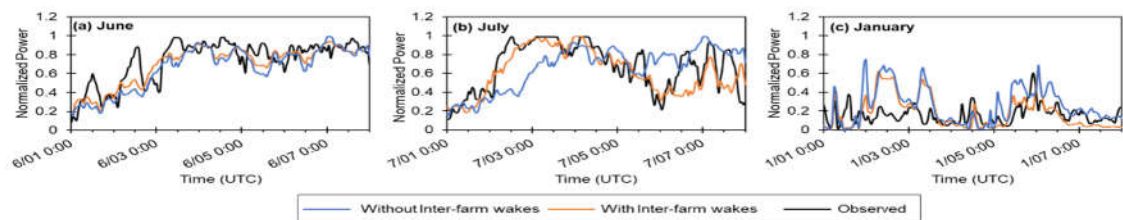


Figure 17. Comparison of forecasted and observed total power generation in FFCEL for the months of (a) June, (b) July, and (c) January

To evaluate the prediction accuracy of the WRF model in determining the total power output of FFCEL, correlation plots are presented in Fig. 18. In these plots, the Pearson correlation coefficient (R) is used to find the extent of linearity between observed and forecasted values. For June and July (Fig. 18(a, b)), R has values of 0.82 and 0.79

respectively presenting a high accuracy of predicted power generation for Case 2. A huge increase in wind power correlation is recorded between forecasted and observed values for July by including the inter-farm wake effects. Conversely, the prediction power of the WRF model drops remarkably in January (Fig. 18(c)) when R has a value of only 0.27 for Case 2.

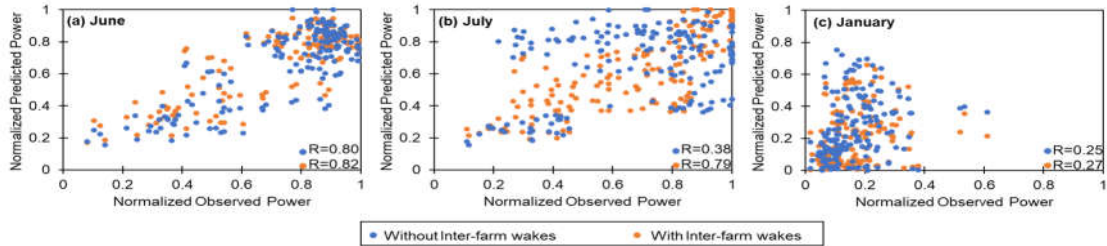


Figure 18. Comparison of predicted and observed total power generation of FFCEL for the months of (a) June, (b) July, and (c) January

The mean value of NMAE (see Fig. 19) for all the turbines for Case 1 is 13% and Case 2 is 11% for June. Improvement of 15% was observed for the mean value of NMAE. A maximum reduction in error for wind power prediction is observed for turbine 28 having a value of 28%. For July, the average value of NMAE for both the cases is approximately 14% and a reduction of 10% in NMAE is observed for turbine 10. Like MAE and RMSE, NMAE is on the higher side in the winter season. The value of NMAE for Case 1 is 19% and Case 2 is 14%, hence a 26% reduction in the mean value was observed for Case 2. A maximum error reduction in prediction is observed for turbine 24, which is 47%. In all the parameters, used to evaluate the accuracy of forecasting skills of the WRF mesoscale model, catering to the inter-farm wakes emerging from the neighboring wind farms decreased the errors and increased forecasting skills.

The discrepancies observed in the power generation emerge from the uncertainties inherent in the WRF mesoscale model. Like other NWP models, the WRF only estimates the atmospheric interaction with the orography of the area by simplifying the physical processes [40]. Errors in the forecasted values also come from the inadequacies of physical parametrization and which leads to the inability of NWP models to successfully solve sub-grid level issues and its skill of interpolation is affected, although it has its error of interpolations. Not selecting the right initial and boundary conditions for the model will also lead to the forecast errors in the NWP models. Errors in wind speed are tripled, when power is predicted in the NWP, because of cubic relation between speed and power. Therefore, a high skill forecasting model is required for the estimation of energy production applications [49]. Typically, bias errors in the wind speed are on the lower side but, if the spatial relationship with the atmospheric interaction is considered, the discrepancies become larger. Another possible cause of errors in results is maybe WRF underestimates wind speeds if mean observed wind speeds are high and overestimates when wind speeds are low.

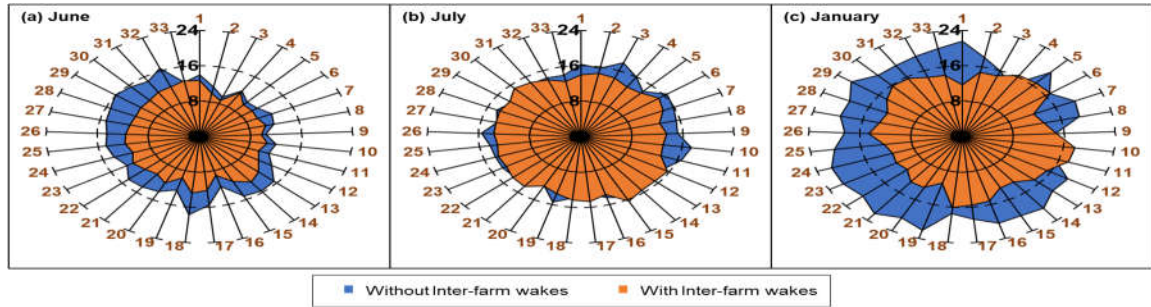


Figure 19. Comparison of normalized mean absolute error values, (NMAE) in %, of power generated by individual turbines for Case 1: without inter-farm wake effects and Case 2: With inter-farm wake effects.

4 Conclusion

In this study, the WRF model integrated with Wind Farm Parameterization (WFP) scheme is used for the wind speed and power forecasting of a utility-scale onshore wind farm which is situated in complex terrain. The forecasted data was compared with the observed data to assess the forecasting skills of the model. The test case wind farm has high occupancy and also experiences wake interference from neighboring wind farms. Furthermore, the wind characteristics of the Jhimpir region, where the wind farms exist, undergo extreme seasonal variations. Main conclusions emerged from this study are:

- Extreme variations in wind characteristics were observed for the current season. During the summer months of June and July, high mean wind speeds from the Arabian sea approach the Jhimpir region from South-West direction. The wind direction is completely reversed during the winter month of January when it approaches the region from the North-East direction. The mean average wind speed during January is also reduced and it exhibits more variability as compared to the summer season. This variation in wind characteristics affected the test-case wind farm's power production and the direction of incoming wake flow.
- In the span of simulations, the WRF overestimated the wind speeds in the summer season, when the mean wind speeds were high. MBE was negative in summer, as the WRF underestimated the inter-farm wake mixing in the downstream wind. The WRF underestimated the wind speed in the winter season and overestimated wakes due to low mean wind speed. The MAE in wind speed for the summer is reduced up to 7.7% by including the inter-farm wakes, while in the winter season, a maximum of 14 % reduction in MAE was observed with the inclusion of inter-farm wake effects.
- Two sets of wind turbines were identified, i.e. set A and set B, in the test-case wind farm based on the wake flow analysis. Set B of wind turbines recorded more influence from upstream wake flows as compared to the set A. A wind speed deficit of more than 12% was found in the set B wind turbines. One wind turbine from each row in both sets of turbines was selected to further analyze the wind

speed and power forecast for two different cases i.e. Case 1: Without inter-farm wakes, and Case 2: With inter-farm wakes. Wind speed and power forecast results close to the observed data were recorded for the selected wind turbines for Case 2. Moreover, a significant reduction in MAE and RMSE was observed in Case 2 for the set B wind turbines as compared to set A. This result bolsters the significance of including the inter-farm wake effects in the forecasting of wind data. Similar to the wind speed, a high correlation between the predicted power values in Case 2 and the observed data was found for summer months. The NMAE for set B wind turbines was also reduced considerably with the inclusion of wake effects.

- The WRF model exhibited lower accuracy during the winter season with high RMSE values in wind speed and high NMAE values in the power output of individual turbines. It can be inferred that the accuracy of the model is dependent on different atmospheric parameters including wind speed. The higher discrepancies in the model’s output during the winter season also emerge from the uncertainties inherent in the atmospheric model, initial and boundary conditions, and over-simplification of physical processes.

Acknowledgments

The authors appreciate the technical and data support provided by the wind companies i.e. the FFCEL, Master Wind Energy, Zorlu, and TGF. The authors would also like to thank the USPCAS-E NUST for providing high-performance computing resources necessary for the successful completion of this study.

| Nomenclature | | | |
|-----------------------|--------------------------------|-------|--|
| Variables | | WRF | Weather Research and Forecasting |
| <i>Obs</i> | Observed values | FFCEL | Fauji Fertilizer Company Energy Limited |
| <i>f</i> | Forecasted values | TGF | Three Gorges wind farm |
| <i>n</i> | Total number of observations | MW | Megawatt |
| <i>dx</i> | Horizontal resolution | GFS | Global Forecasting System |
| <i>dy</i> | Vertical resolution | NCEP | National Center for Environmental Prediction |
| <i>R</i> ₁ | Pearson Correlation for Case 1 | MODIS | Moderate Imaging Spectroradiometer |
| <i>R</i> ₂ | Pearson Correlation for Case 2 | MYNN | Mellor–Yamada Nakanishi Niino |
| | | PBL | Planetary boundary layer |
| Acronyms | | MAE | Mean Absolute Error |
| GW | Gigawatt | MBE | Mean Bias Error |
| CFD | Computational Fluid Dynamics | RMSE | Root Mean Square Error |

| | | | |
|-----|------------------------------|------|---------------------------------|
| NWP | Numerical Weather Prediction | NMAE | Normalized Mean Absolute Error |
| MM5 | Mesoscale Model | R | Pearson Correlation Coefficient |
| LES | Large-eddy Simulation | UTC | Coordinated Universal Time |

References

- [1] IRENA, *Renewable Energy Statistics 2019*, vol. 1, no. 1. 2019.
- [2] S. S. Soman, H. Zareipour, O. Malik, and P. Mandal, "A review of wind power and wind speed forecasting methods with different time horizons," *North Am. Power Symp. 2010, NAPS 2010*, 2010.
- [3] E. A. Bossanyi, "Short-Term Wind Prediction Using Kalman Filters," *Wind Eng.*, vol. 9, no. 1, pp. 1–8, 1985.
- [4] A. Sfetsos, "A novel approach for the forecasting of mean hourly wind speed time series," *Renew. Energy*, vol. 27, no. 2, pp. 163–174, 2002.
- [5] M. Mohandes, S. Rehman, and T. O. Halawani, "Estimation of global solar radiation using artificial neural networks," *Renew. Energy*, vol. 14, no. 1–4, pp. 179–184, 1998.
- [6] A. Alexandridis and A. Zapranis, "Wind Derivatives: Modeling and Pricing," *Comput. Econ.*, vol. 41, no. 3, pp. 299–326, 2013.
- [7] M. Monfared, S. K. Y. Nikraves, and H. Rastegar, "A Novel Fuzzy Predictor for Wind Speed," *Lect. Notes Eng. Comput. Sci.*, vol. 2167, no. 1, pp. 840–843, 2007.
- [8] A. R. Daniel and A. A. Chen, "Stochastic simulation and forecasting of hourly average wind speed sequences in Jamaica," *Sol. Energy*, vol. 46, no. 1, pp. 1–11, 1991.
- [9] profil kesehatan indonesia, "Provil Kesehatan Indonesia 2018," vol. 16, p. 496, 2018.
- [10] P. P. Craig, A. Gadgil, and J. G. Koomey, "What Can History Teach Us? A Retrospective Examination of Long-Term Energy Forecasts for the United States," *Annu. Rev. Energy Environ.*, vol. 27, no. 1, pp. 83–118, 2002.
- [11] G. Giebel and L. Landberg, "State-of-the-Art on Methods and Software Tools for Short-Term Prediction of Wind Energy Production," *Energy*, pp. 16–19, 2010.
- [12] C. W. Potter and M. Negnevitsky, "Very short-term wind forecasting for Tasmanian power generation," *IEEE Trans. Power Syst.*, vol. 21, no. 2, pp. 965–972, 2006.
- [13] L. Landberg, "A mathematical look at a physical power prediction model," *Wind Energy*, vol. 1, no. 1, pp. 23–28, 1998.

- [14] S. Al-Yahyai, Y. Charabi, and A. Gastli, "Review of the use of numerical weather prediction (NWP) models for wind energy assessment," *Renew. Sustain. Energy Rev.*, vol. 14, no. 9, pp. 3192–3198, 2010.
- [15] K. Solbakken and Y. Birkelund, "Evaluation of the Weather Research and Forecasting (WRF) model with respect to wind in complex terrain," *J. Phys. Conf. Ser.*, vol. 1102, p. 12011, Oct. 2018.
- [16] A. J. Deppe, W. A. Gallus, and E. S. Takle, "A WRF ensemble for improved wind speed forecasts at turbine height," *Weather Forecast.*, vol. 28, no. 1, pp. 212–228, 2013.
- [17] M. Bilal, K. Solbakken, and Y. Birkelund, "Wind speed and direction predictions by WRF and WindSim coupling over Nygårdstjøll," *J. Phys. Conf. Ser.*, vol. 753, no. 8, 2016.
- [18] B. Efe *et al.*, "72hr forecast of wind power in Manisa, Turkey by using the WRF model coupled to WindSim," *2012 Int. Conf. Renew. Energy Res. Appl. ICRERA 2012*, pp. 1–6, 2012.
- [19] Y. Che, X. Peng, L. Delle Monache, T. Kawaguchi, and F. Xiao, "A wind power forecasting system based on the weather research and forecasting model and Kalman filtering over a wind-farm in Japan," *J. Renew. Sustain. Energy*, vol. 8, no. 1, 2016.
- [20] G. Martínez-Arellano and L. Nolle, "Short-term wind power forecasting with WRF-ARW model and genetic programming," *Mendel*, pp. 51–56, 2013.
- [21] D. C. Li, C. J. Chang, C. C. Chen, and W. C. Chen, "Forecasting short-term electricity consumption using the adaptive grey-based approach—An Asian case," *Omega*, vol. 40, no. 6, pp. 767–773, 2012.
- [22] M. Magnusson and A.-S. Smedman, "A Practical Method to Estimate Wind Turbine Wake Characteristics from Turbine Data and Routine Wind Measurements," *Wind Eng.*, vol. 20, no. 2, pp. 73–92, Feb. 1996.
- [23] M. F. Howland, S. K. Lele, and J. O. Dabiri, "Wind farm power optimization through wake steering," *Proc. Natl. Acad. Sci.*, vol. 116, no. 29, pp. 14495–14500, 2019.
- [24] M. A. Prósper, C. Otero-Casal, F. C. Fernández, and G. Miguez-Macho, "Wind power forecasting for a real onshore wind farm on complex terrain using WRF high resolution simulations," *Renew. Energy*, vol. 135, pp. 674–686, 2019.
- [25] J. K. Lundquist, K. K. DuVivier, D. Kaffine, and J. M. Tomaszewski, "Costs and consequences of wind turbine wake effects arising from uncoordinated wind energy development," *Nat. Energy*, vol. 4, no. 1, pp. 26–34, 2019.
- [26] L. Li, Y. M. Wang, and Y. Q. Liu, "Impact of wake effect on wind power prediction," *IET Conf. Publ.*, vol. 2013, no. 623 CP, pp. 20–23, 2013.

- [27] C. L. Archer *et al.*, “Review and evaluation of wake loss models for wind energy applications,” *Appl. Energy*, vol. 226, no. May 2018, pp. 1187–1207, 2018.
- [28] S. Jeon, B. Kim, and J. Huh, “Comparison and verification of wake models in an onshore wind farm considering single wake condition of the 2 MW wind turbine,” *Energy*, vol. 93, pp. 1769–1777, 2015.
- [29] X. Gao, H. Yang, and L. Lu, “Optimization of wind turbine layout position in a wind farm using a newly-developed two-dimensional wake model,” *Appl. Energy*, vol. 174, pp. 192–200, 2016.
- [30] S. Frandsen *et al.*, “Analytical modelling of wind speed deficit in large offshore wind farms,” *Wind Energy*, vol. 9, no. 1–2, pp. 39–53, 2006.
- [31] Y. Wang, W. Miao, Q. Ding, C. Li, and B. Xiang, “Numerical investigations on control strategies of wake deviation for large wind turbines in an offshore wind farm,” *Ocean Eng.*, vol. 173, no. December 2018, pp. 794–801, 2019.
- [32] J. Kuo, D. Rehman, D. A. Romero, and C. H. Amon, “A novel wake model for wind farm design on complex terrains,” *J. Wind Eng. Ind. Aerodyn.*, vol. 174, no. January, pp. 94–102, 2018.
- [33] X. Yang, M. Pakula, and F. Sotiropoulos, “Large-eddy simulation of a utility-scale wind farm in complex terrain,” *Appl. Energy*, vol. 229, no. May, pp. 767–777, 2018.
- [34] A. C. Fitch *et al.*, “Local and mesoscale impacts of wind farms as parameterized in a mesoscale NWP model,” *Mon. Weather Rev.*, vol. 140, no. 9, pp. 3017–3038, 2012.
- [35] W. C. Skamarock *et al.*, “A Description of the Advanced Research WRF Model Version 4 NCAR Technical Note,” *Natl. Cent. Atmos. Res.*, p. 145, 2019.
- [36] T. Prabha and G. Hoogenboom, “Evaluation of the Weather Research and Forecasting model for two frost events,” *Comput. Electron. Agric.*, vol. 64, no. 2, pp. 234–247, 2008.
- [37] M. Amjad, Q. Zafar, F. Khan, and M. M. Sheikh, “Evaluation of weather research and forecasting model for the assessment of wind resource over Gharo, Pakistan,” *Int. J. Climatol.*, vol. 35, no. 8, pp. 1821–1832, 2015.
- [38] J. G. Powers *et al.*, “The weather research and forecasting model: Overview, system efforts, and future directions,” *Bull. Am. Meteorol. Soc.*, vol. 98, no. 8, pp. 1717–1737, 2017.
- [39] Pedro A. Jimenez, “10 jamCd120266 1610..1617.pdf.”.
- [40] D. Carvalho, A. Rocha, C. S. Santos, and R. Pereira, “Wind resource modelling in complex terrain using different mesoscale-microscale coupling techniques,” *Appl. Energy*, vol. 108, pp. 493–504, 2013.

- [41] A. Haseeb, R. M. Asim, A. Javed, and R. Calhoun, “Partial Repowering Analysis of a Wind Farm by Turbine Hub Height Variation to Mitigate Neighboring Wind Farm Wake Interference using Mesoscale Simulations,” *Appl. Energy*, vol. 268, no. April, pp. 1–23, 2020.
- [42] A. Jabbari, J.-M. So, and D.-H. Bae, “Accuracy assessment of real-time flood forecasting of coupled hydrological and mesoscale meteorological models,” *Nat. Hazards Earth Syst. Sci. Discuss.*, no. January, pp. 1–36, 2018.
- [43] T. T. Warner, “Quality assurance in atmospheric modeling,” *Bull. Am. Meteorol. Soc.*, vol. 92, no. 12, pp. 1601–1610, 2011.
- [44] M. J. Iacono, J. S. Delamere, E. J. Mlawer, M. W. Shephard, S. A. Clough, and W. D. Collins, “Radiative forcing by long-lived greenhouse gases: Calculations with the AER radiative transfer models,” *J. Geophys. Res. Atmos.*, vol. 113, no. D13, 2008.
- [45] G. Thompson, P. R. Field, R. M. Rasmussen, and W. D. Hall, “Explicit Forecasts of Winter Precipitation Using an Improved Bulk Microphysics Scheme. Part II: Implementation of a New Snow Parameterization,” *Mon. Weather Rev.*, vol. 136, no. 12, pp. 5095–5115, 2008.
- [46] Z.-L. Yang *et al.*, “The community Noah land surface model with multiparameterization options (Noah-MP): 2. Evaluation over global river basins,” *J. Geophys. Res. Atmos.*, vol. 116, no. D12, Jun. 2011.
- [47] M. NAKANISHI and H. NIINO, “Development of an Improved Turbulence Closure Model for the Atmospheric Boundary Layer,” *J. Meteorol. Soc. Japan. Ser. II*, vol. 87, no. 5, pp. 895–912, 2009.
- [48] C. Zhang, Y. Wang, and K. Hamilton, “Improved Representation of Boundary Layer Clouds over the Southeast Pacific in ARW-WRF Using a Modified Tiedtke Cumulus Parameterization Scheme,” *Mon. Weather Rev.*, vol. 139, no. 11, pp. 3489–3513, 2011.
- [49] F. Cassola and M. Burlando, “Wind speed and wind energy forecast through Kalman filtering of Numerical Weather Prediction model output,” *Appl. Energy*, vol. 99, pp. 154–166, 2012.